# Regional exhumation history of brittle crust during subduction initiation, Fiordland, southwest New Zealand, and implications for thermochronologic sampling and analysis strategies

**Rupert Sutherland***
*GNS Science (Institute of Geological and Nuclear Sciences), P.O. Box 30-368, Lower Hutt, New Zealand*

**Michael Gurnis***
*Seismological Laboratory, California Institute of Technology, Pasadena, California 91125, USA*

**Peter J. J. Kamp***
*Department of Earth Sciences, University of Waikato, Hamilton, New Zealand*

**Martha A. House***
*Natural Sciences Division, Pasadena City College, 1570 East Colorado Boulevard, Building E, Room 210, Pasadena, California 91106, USA*

## ABSTRACT

We analyze spatial trends and statistical properties of 410 apatite and zircon fission track and (U-Th)/He ages, and implement a weighted least-squares regression scheme to obtain the regional rock uplift history associated with subduction initiation beneath Fiordland, New Zealand. We observe the onset of rapid exhumation at 25–15 Ma in southwest Fiordland, immediately following a time of significant change in regional plate motions. During the period 15–5 Ma, the locus of rapid exhumation broadened and migrated toward the northeast at ~30% of the plate motion rate, but exhumation remained localized along the northwest margin. Since 5 Ma, the zone of rapid exhumation has become broader, and the present high-amplitude gravity and topographic anomalies are spatially associated with the most tightly folded part of the subducted slab. We suggest that the pattern of exhumation tracks the along-strike and downdip development of the subducted slab, which requires tectonic erosion of mantle lithosphere of the overriding plate. Based upon local patterns of age variability, we hypothesize that brittle faults have displaced and rotated equal-cooling-age surfaces, and that there is short-wavelength (<10 km) spatial correlation between faults and topographic features. Our regression method allows us to simultaneously consider implications of all age data, evaluate "geological noise" introduced by brittle faults, and make cooling age predictions at any point in the region. The residuals from our regression indicate that, on average, mountain tops in Fiordland have undergone slightly greater rock uplift than adjacent valleys, even though our data are too sparse to identify specific faults. We suggest that sampling programs in active tectonic settings such as Fiordland must be sufficiently dense to determine both mean exhumation history and regional geological variability associated with faults.

## INTRODUCTION

The cooling history of certain minerals can be constrained using thermochronologic analyses that are based upon production and diffusion of noble gases, or rates of fission track creation and annealing. Model cooling ages derived from these observations are commonly used to test thermal predictions from deformation and rock uplift models. While a well-constrained cooling history derived from an individual rock may, in some circumstances, be sufficient to test the hypothesis in question, spatial variations in cooling ages are more usually required to test useful geological models. The spatial distribution of data generally complicates any such analysis because it may not be logistically feasible to collect samples in optimal locations; suitable rock types may not be exposed; relevant data from previous studies may have been collected for different purposes; and limited funds or laboratory facilities usually limit spatial coverage.

The hypotheses we wish to test relate to the process of subduction zone initiation beneath southwestern New Zealand (Fig. 1). The location is globally significant because it is one of the few places on Earth where an active, nascent, and isolated subduction zone can be studied (Gurnis et al., 2004). Oblique convergence during Miocene–Quaternary time has resulted in subduction of Eocene–Miocene ocean crust at the Puysegur Trench and formation of the Alpine fault (Barnes et al., 2005; Christoffel and van der Linden, 1972; Davey and Smith, 1983; Delteil et al., 1996; Lamarche and Lebrun, 2000; Lebrun et al., 2003; Sutherland et al., 2000).

The subducted slab is twisted beneath Fiordland (Fig. 2), with geometry reminiscent of an inverted ploughshare (Christoffel and van der Linden, 1972; Eberhart-Phillips and Reyners, 2001; Reyners et al., 2002). High-amplitude gravity and topographic anomalies exist at both the southern and northern ends of the subduction zone (Fig. 2), and the central part of the zone (47–49°S) is characterized by lower amplitude anomalies and Quaternary subsidence (Collot et al., 1995; Lamarche and Lebrun, 2000). Distributed lithospheric strain that accumulated farther east, within the overriding plate, has bent geologic markers into an orocline, caused crustal thickening and uplift, and resulted in a high-seismic-velocity lithospheric root (Fig. 2) (Eberhart-Phillips and Reyners, 2001; Norris, 1979; Sutherland, 1999). Three young

*Emails: Sutherland: r.sutherland@gns.cri.nz; Gurnis: gurnis@caltech.edu; Kamp: p.kamp@waikato.ac.nz; House: mahouse@pasadena.edu.
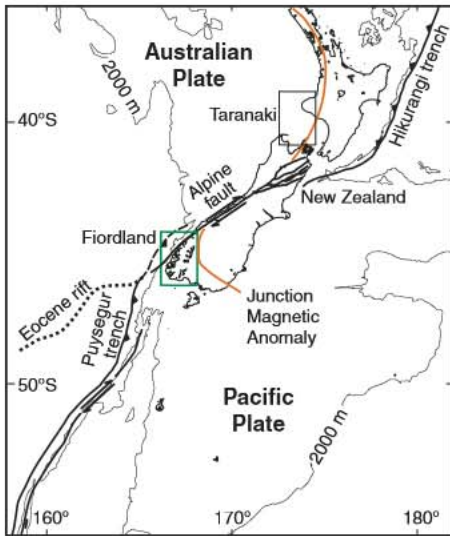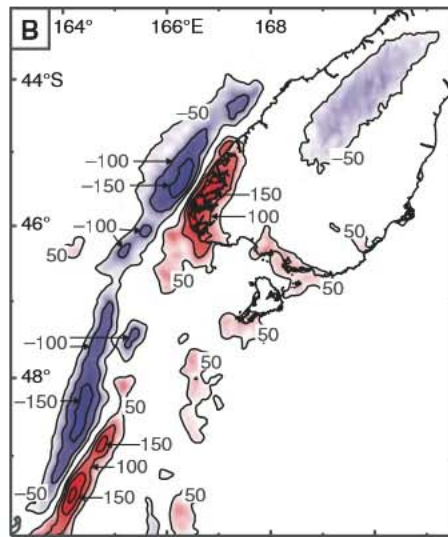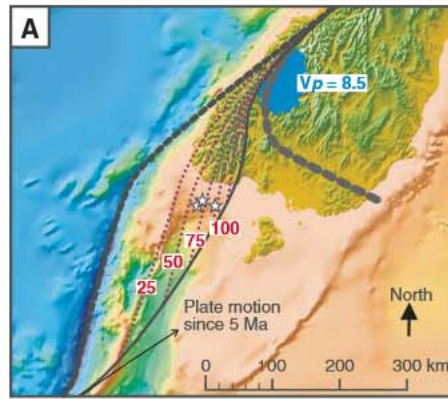
Figure 1. Location of the Puysegur-Fiordland oblique subduction zone and the Alpine fault in New Zealand, southwest Pacific. The Eocene rift margin separates Australian plate continental crust of western New Zealand and Tasman Sea oceanic crust from Eocene–Miocene oceanic crust farther south (Lamarche et al., 1997; Wood et al., 1996); the Alpine fault is close to this boundary and was created as buoyant continental crust collided, whereas Eocene–Miocene oceanic crust was subducted at the Puysegur Trench (Sutherland et al., 2000). The Junction magnetic anomaly (red line) follows Mesozoic basement rock fabric, which has been bent into an orocline during Cenozoic deformation (Sutherland, 1999).



Figure 2. A) Structural contours (depths in km) on the top of the subducted slab inferred from earthquake and active-source seismology (Eberhart-Phillips and Reyners, 2001; Melhuish et al., 1999; Reyners et al., 2002); stars show the locations of late Cenozoic arc volcanoes (Reay and Parkinson, 1997; Sutherland et al., 2006a); the blue region has anomalously high V*p* of >8.5 km/s at 100 km depth (Eberhart-Phillips and Reyners, 2001). B) High-amplitude paired gravity anomalies exist at the southern and northern ends of the Fiordland subduction zone; free-air anomalies are shown offshore and Bouger anomalies onshore.

(younger than 5 Ma; probably younger than 2 Ma) and small arc volcanoes exist (Fig. 2), though none are thought to be active (Reay and Parkinson, 1997; Sutherland et al., 2006a).

There is currently a strong spatial correlation between where the subducted slab is being twisted downward and the high topography and positive gravity anomalies of Fiordland (Fig. 2). We hypothesize that this correlation is causally related to the geodynamic setting and that a similar relationship existed in the past (House et al., 2002); hence we use the rock cooling response, caused by exhumation and the emplacement of a slab, and recorded using thermochronology, to track the spatial evolution of the subduction zone.

In our first paper (House et al., 2002) we presented a preliminary data set of 32 apatite (U-Th)/He and 34 apatite fission track ages, showed that thermochonology data could be used to track the evolution of subduction, and presented a hypothesis for how and why

exhumation occurred above the developing subduction zone. In our second paper (House et al., 2005) we presented a further 28 apatite (U-Th)/He and 6 zircon (U-Th)/He ages, which increased the geographic coverage, and showed that zircon data provide an essential constraint on the timing of subduction initiation in central and western Fiordland.

In this paper we analyze spatial trends and statistical properties of a much larger data set, which is made up of 66 apatite (U-Th)/He, 210 apatite fission track, 6 zircon (U-Th)/He, and 128 zircon fission track ages (see Supplemental File 1[1]); and we also use published K/Ar data. The fourfold increase in the number of data and the inclusion of 128 zircon fission track ages for the first time allows us to reliably determine the subduction-related exhumation distribution and history for the entire region. We consider the statistical properties of the data set and implement a new analysis method: a weighted least-squares regression scheme that allows us to obtain the regional rock uplift history and a quantitative measure of uncertainty surrounding that history. The observations, method, and results have implications for subduction initiation geodynamics, the mechanisms of exhumation and cooling of brittle crust at plate boundaries, and future collection and analysis strategies for thermochronologic data.

## SPATIAL VARIATION IN COOLING AGE: THEORETICAL CONSIDERATION

Consider two very precisely determined cooling ages, $A_i$ and $A_j$, of the same type at distinct locations $i$ and $j$ within a scalar age field $A$. The age difference, $\delta A_{ij}$, is caused by continuous variation along a path between the two points, and discontinuous changes in age across faults:

$$\delta A_{ij} = A_j - A_i = \int_v \nabla A \cdot ds - \sum_k \int_{u_k} \nabla A \cdot ds \quad (1)$$

The vector **v** is the direct path between $i$ and $j$, and the set of path vectors $\{u_k\}$ is defined by the offsets in equal-age surfaces at each of the $k$ faults that are crossed by **v** (Fig 3). The term $\nabla A \cdot ds$ is the vector dot product between the gradient of the age field and the path vector.

In practice, most sampling is done over a relatively narrow vertical interval, because topographic variations are usually small compared to horizontal distances, i.e., **v** usually has a shallow inclination. A positive correlation between age and altitude is expected for nearby samples with no faults between them, because isotherms at depth are close to horizontal and ages are frozen into the rock as uplift and exhumation occurs, i.e., $\nabla A$ is usually steeply inclined upward; and the magnitude of the spatial age gradient, $\|\nabla A\|$, is closely related to the cooling rate during the period the age became frozen into the rock,

---

making it a useful quantity to analyze (Benjamin et al., 1987; Ehlers, 2005; Fitzgerald, 1994; House et al., 2002, 1998).

It may be useful to assume that the equal age surfaces have a mean dip, $\theta$, in which case, age variation takes the approximate form

$$\delta A_{ij} =$$

$$\left( x_{ij} \tan\theta \sin\phi + z_{ij} + \sum_k \zeta_k \right) \left\| \nabla A_{ij} \right\| \cos\theta \quad (2)$$

where, evaluated along a direct path between $i$ and $j$, $x_{ij}$ is the horizontal separation, $\phi$ is the angle between the direction traveled and the mean strike of equal-age surfaces, $z_{ij}$ is the vertical separation, $\zeta_k$ is the vertical throw on the $k^{th}$ fault crossed, and $\left\| \nabla A_{ij} \right\|$ is the magnitude of the mean spatial age gradient at points along the path.

The expected value of the square of the measured age difference between two nearby points is

$$E\left[ \delta A_{ij}^2 \right] = \sigma_i^2 + \sigma_j^2 + \varepsilon_{ij}^2 \quad (3)$$

where $\sigma_i$ and $\sigma_j$ are the known standard errors associated with each age measurement and $\varepsilon_{ij}^2$ is a remainder term. We consider a model for the remainder that has the form

$$\varepsilon_{ij}^2 = a + b x_{ij} + c^2 x_{ij}^2 \quad (4)$$

$$c \approx \left\| \nabla A_{ij} \right\| \sin\theta \sin\phi \quad (5)$$

The constant $a$ relates to measurement uncertainty associated with natural variations in helium diffusivity or fission track annealing
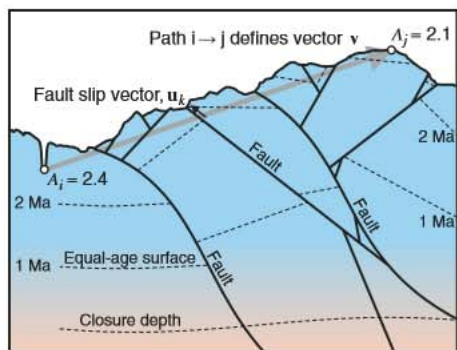
kinetics (mostly related to fluorine content in apatite), radiation distribution (crystal zoning and inclusions), or morphology of the crystals, or other uncertainty introduced by analytical procedures that is not included in the quoted precision. The term $b x_{ij}$ is a random walk component associated with faulting and topography. The term $c^2 x_{ij}^2$ is a first approximation for the age variance introduced by an underlying spatial trend within the age field.

## OBSERVED VARIATIONS OF COOLING AGE IN FIORDLAND

### Data Set

Our data set (Fig. 4; Supplemental File 1 [see footnote 1]) includes 66 apatite (U-Th)/He ages (AHE), 210 apatite fission track ages (AFT), 6 zircon (U-Th)/He ages (ZHE), 128 zircon fission track ages (ZFT), and 8 white mica



Figure 3. Geological cross section between two thermochronologic age determinations $A_i$ and $A_j$. The age difference is the sum of the continuous variation along a direct path between the sites, which defines the vector **v**, and the discontinuous age differences that result from fault offsets defined by the $k$ slip vectors $\{\mathbf{u}_k\}$.
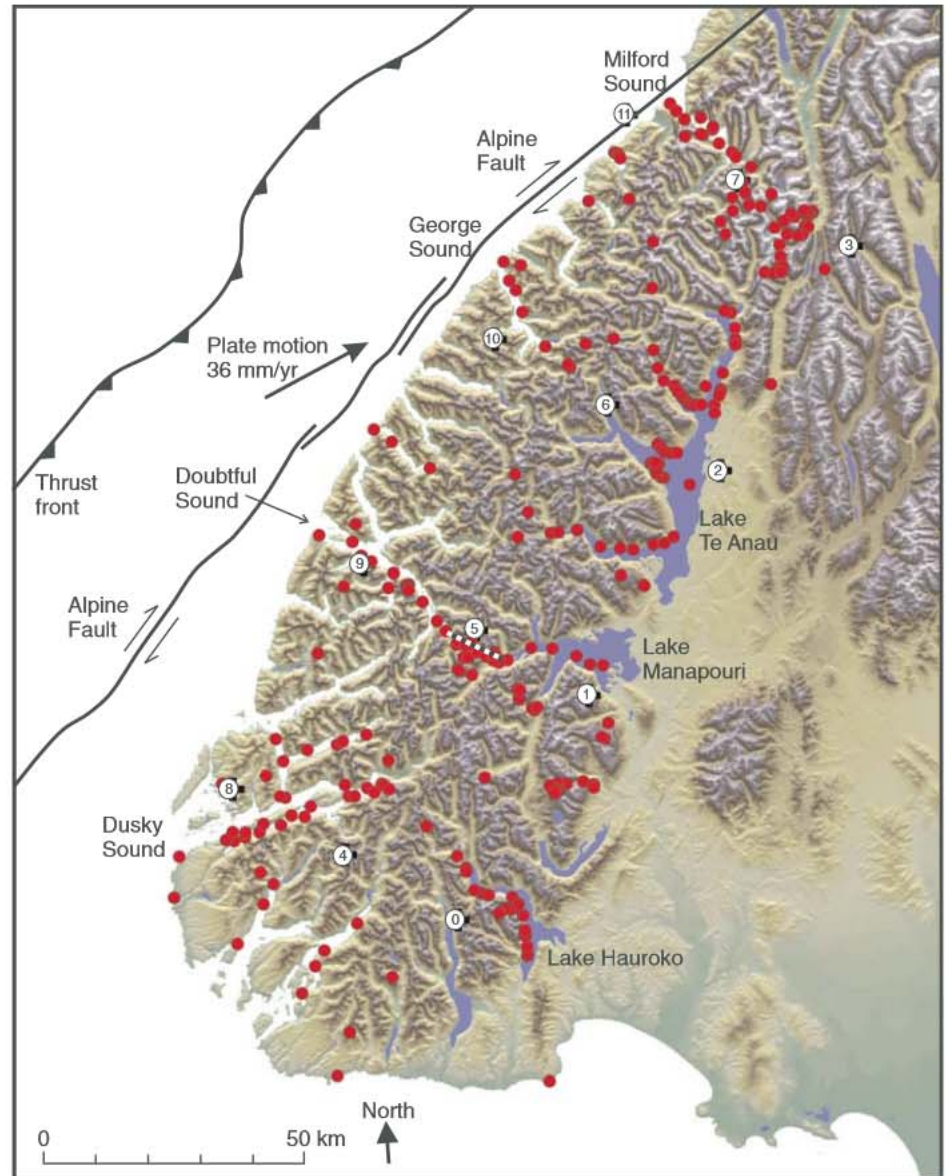


Figure 4. Shaded and colored digital-terrain model of Fiordland. Typical peak heights are in the range 1000–2000 m; the highest topography (2800 m) is inland from Milford Sound. Sample locations (red circles) and model grid nodes (numbered) are shown. The Manapouri tunnel (black and white short dashes near node 5) crosses central Fiordland close to sea level between Lake Manapouri and Doubtful Sound. Nuvel-1A plate motion (DeMets et al., 1994) is highly oblique to the Alpine fault, which accommodates 20–30 mm/yr of pure strike-slip displacement (Barnes et al., 2005; Sutherland et al., 2006b).

K/Ar ages from near Milford Sound (Claypool et al., 2002; House et al., 2002, 2005). The K/Ar and U/Pb ages from Fiordland are at least Cretaceous (Nathan et al., 2000), which is older than the time of interest, except in the coastal region near Milford Sound, where published white mica K/Ar ages are Neogene (Claypool et al., 2002).

### Spatial Trends in Age and Age-Altitude Correlation

The age difference and spatial relationships for every age pair of the same type in the Fiordland data set were computed, and results were sorted by separation distance. Based upon previous work (House et al., 2002; Sutherland et al., 2006a; Turnbull and Uruski, 1993), we separated two subgroups of age pairs for each age type on the basis of mean age: ages younger than 10 Ma are inferred to have been frozen into the rock during relatively rapid exhumation and cooling associated with subduction initiation; ages older than 20 Ma are generally inferred to predate the most active tectonic phase and are likely to have cooled at a significantly slower rate through their respective closure temperatures.

Age-altitude correlations (Fig. 5) were assessed by examining age pairs that had relatively small horizontal separations of <3 km and a difference in altitude of >100 m. For samples with horizontal spacing <1.5 km, weak positive correlations are observed for AHE younger than 10 Ma, AFT older than 20 Ma, and ZFT older than 20 Ma. The correlation is noticeably weaker when samples separated by <3 km are considered. The presence of highly variable age-altitude gradients and significant outliers (i.e., age decreases with altitude for some age pairs), combined with the weak (AHE younger than 10 Ma; AFT older than 20 Ma; ZFT older than 20 Ma) or undetectable (AFT younger than 10 Ma) correlation between age and altitude within the data set, suggests that local faulting and block rotations are widespread in Fiordland: the distance between significant faults is inferred to be commonly <3 km.

We note, however, that if we consider the data set as a whole by binning and averaging all data by altitude, then the weak positive correlation observed from individual pairs (Fig. 5: AHE younger than 10 Ma; AFT older than 20 Ma; ZFT older than 20 Ma) can be better quantified (see Supplemental File 1 [see footnote 1]).

### Spatial Trends in Age Variance: Geological Noise

A strong linear correlation is observed (Fig. 6) between the square of the age difference and the square of the separation distance (see
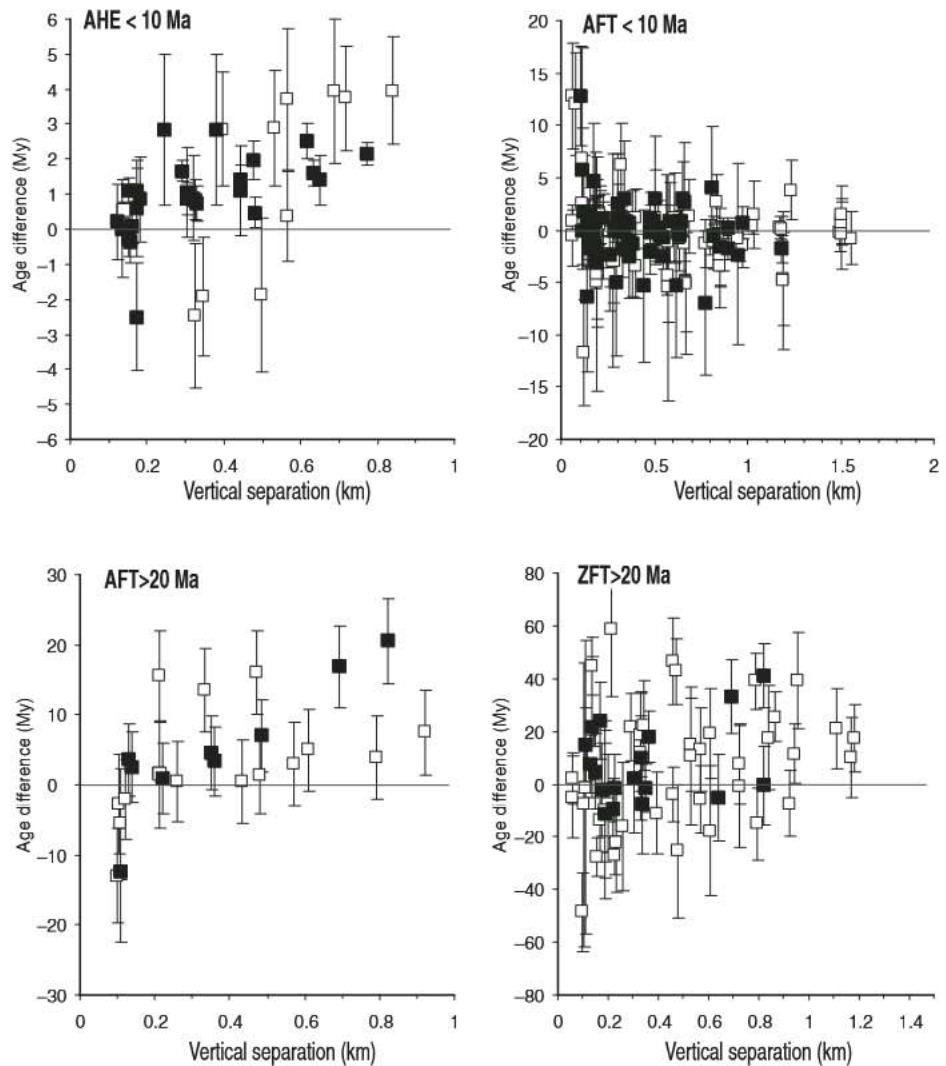


Figure 5. Age difference plotted against vertical separation (altitude) difference for each age pair horizontally separated by <3 km (open squares) and <1.5 km (filled squares). Age difference uncertainties are inferred 95% confidence limits. AHE—Apatite (U-Th)/He; AFT—apatite fission track; ZFT—zircon fission track.

equations 3 and 4). This is consistent with the observation that the data set displays relatively smooth spatial changes in age over distances of 10–100 km. For AFT and ZFT age pairs with mean age older than 20 Ma, the squared age difference for samples separated by <10 km is significantly underestimated by a linear model, indicating that the $bx_{ij}$ term (equation 4) is significant at these small offsets. We conclude that $b$ is a function of $x_{ij}$: $b$ tends to a constant value at small values of $x_{ij}$, but $bx_{ij}$ tends to a constant value at large values of $x_{ij}$ (>10 km). We suggest that this is because the true difference in exhumation over large distances is modulated by lithospheric and crustal dynamics and varies smoothly. Note that older ages are from regions that have undergone less total exhumation and

are located in eastern Fiordland, farthest from the Alpine fault.

The slope of the linear regression lines is much greater for data pairs with mean age older than 20 Ma than it is for data pairs with mean age younger than 10 Ma (Fig. 6). This follows from previous geological work, which shows that exhumation and cooling rates were much higher during the later period (producing a lower spatial age gradient), and the observation that the slope of the regression line is dependent upon the square of the magnitude of the spatial age gradient, $\|\nabla A\|$ (see equation 5).

The intercept values of the linear regression lines demonstrate that the geological contribution to age variance between sites is substantially larger than the contribution from analytical

uncertainties, even over small distances (<3 km). We can further quantify this "geological noise," which we define as the geological contribution to age variance, by considering the y axis intercept values and subtracting the contribution from known analytical uncertainty (equations 3–5; Fig. 6). For AHE data pairs with mean age younger than 10 Ma the value is 2.3 My$^2$ (Fig. 6), which is equivalent to a mean accumulated throw of 0.5 km, as determined from the mean age gradient of 3.0 My/km (Fig. S1 in Supplemental File 1 [see footnote 1]). For AFT data pairs with mean age older than 20 Ma, a value of 1527 My$^2$ and age gradient of 11.8 My/km (Fig. S1) gives a mean throw of 3.3 km. For ZFT data pairs with mean age older than 20 Ma, a value of 770 My$^2$ and age gradient of 16.3 My/km (Fig. S1 in Supplemental File 1 [see footnote 1]) gives a mean accumulated throw of 1.7 km. This mean accumulated throw is an estimate of the standard deviation of the sum of the throws on all the faults between two sites, after the throw associated with continuous variation is removed. Although these independent calculations yield similar results, we reiterate that the uncertainties are large, because correlations between age and elevation are highly uncertain (Fig. 5) and dependent upon a number of assumptions that are dealt with more thoroughly in the following.

## Temporal Changes in Age Variance and Inferred Exhumation Rate

By taking age pairs with horizontal separation <10 km, we are able to analyze the variance of age pairs as a function of mean age. We have plotted the square root of the mean squared age difference (RMS) as a function of age (Fig. 7), because we infer (from equation 5), that this quantity is linearly related to the magnitude of the spatial age gradient, and hence approximately inversely related to the exhumation rate at the age of cooling. The AFT data set is large and many AFT ages span the time of interest, so it was subdivided into north, central, and southern groups.

ZFT data have high RMS age difference for times before 18–20 Ma (Fig. 7), suggesting slow rates of cooling before 20 Ma. ZFT ages of ca. 16 Ma are most prevalent in the Doubtful Sound region. A small group of ZFT samples from near Milford Sound have elevated RMS age difference values with mean age 12–14 Ma, suggesting a later onset of rapid cooling in that region. The time of onset of low AFT RMS age difference values becomes younger toward the north, suggesting a progressive northward onset of rapid exhumation over the period 16–6 Ma.

If exhumation rate were spatially variable, but not temporally variable, and geological noise
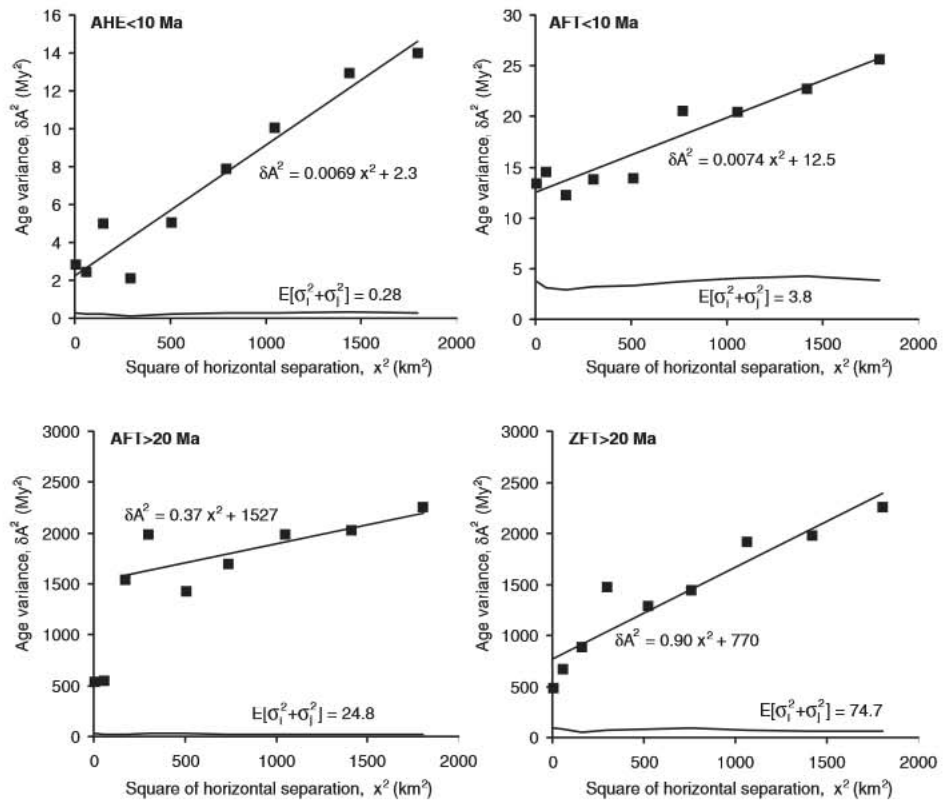


Figure 6. Mean value of the squared age difference, $\delta A^2_{ij}$, plotted as a function of squared separation distance. AHE—Apatite (U-Th)/He; AFT—apatite fission track; ZFT—zircon fission track. The variance component associated with quoted measurement uncertainty is shown as a solid line and the mean value annotated ($E[\sigma_i^2 + \sigma_j^2]$).
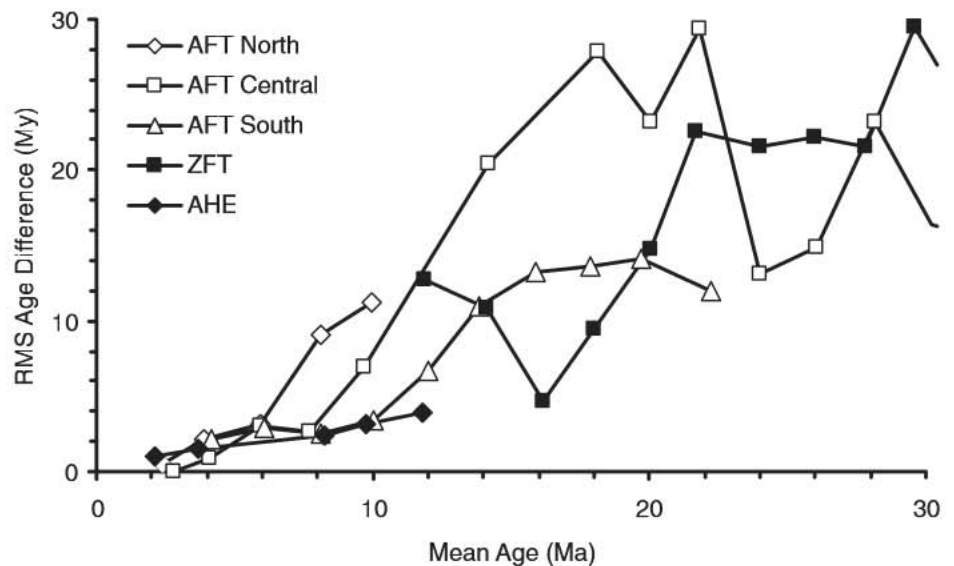


Figure 7. Square root of the mean squared age difference (RMS) of samples separated by <10 km, plotted as a function of mean age. Low values of RMS age difference indicate that cooling was more rapid at that time (see main text). AHE—Apatite (U-Th)/He; AFT—apatite fission track; ZFT—zircon fission track.

were similar everywhere, then the RMS age difference values should plot approximately on a straight line that passes through the origin. It is clear from Figure 7 that many apatite data are close to a straight line that passes through the origin; the slope of the line is 0.3–0.5. Assuming a closure depth of 3–6 km, this implies an accumulated mean throw between samples in the range 0.9–3.0 km. However, it is also clear that all of the data cannot be solely explained by geological noise and temporally-constant, but by spatially-variable rock uplift.

## SCHEME FOR DETERMINING A BEST-FIT REGIONAL ROCK UPLIFT HISTORY

It is clear from our spatial analysis of the data set (above) that a coherent spatial signal over distances of >10 km is embedded in the data set, and that analytical uncertainty is not sufficient to explain observed age variations over even quite small separations of <3 km. We wish to find a model of regional rock uplift history that best reproduces a set of $n$ cooling ages $\{A_i\}$ of different types and known standard errors $\{\sigma_i\}$, and we would like an estimate for the range of possible models. We choose to implement a weighted least-squares regression scheme that takes into account both analytical uncertainties and geological noise; the model parameterization and assumptions are tailored to the geological hypotheses being tested and the data distribution.

The scheme proceeds as follows (Fig. 8): a rock uplift history is defined from a set of parameters (initially guessed) at each node within a regular spatial grid; a rock uplift history is interpolated at each datum; a thermal history is computed at each datum; a model age is computed at each datum; a residual rock uplift value and effective cooling depth are determined at each datum by perturbing the rock uplift history (and hence thermal history) until the model age matches the observed age (Fig. 9); a parameter search is conducted to find a new regional uplift history that better matches the effective cooling depths and cooling ages; the original parameters are adjusted to be closer to the best parameters found during the search; and the procedure is restarted. The scheme is complete when no improvement (at some specified precision) is found during the parameter search.

We choose a parameterization for the rock uplift history that suits the hypotheses we wish to test: how much total rock uplift has occurred; when did uplift start; and how has the rate of rock uplift changed during the past 5 My? We require three parameters: an initial depth, an age of inception (older than 5 Ma) for rock uplift and exhumation, and a rock uplift



Figure 8. Flow chart illustrating the regression strategy (see text).
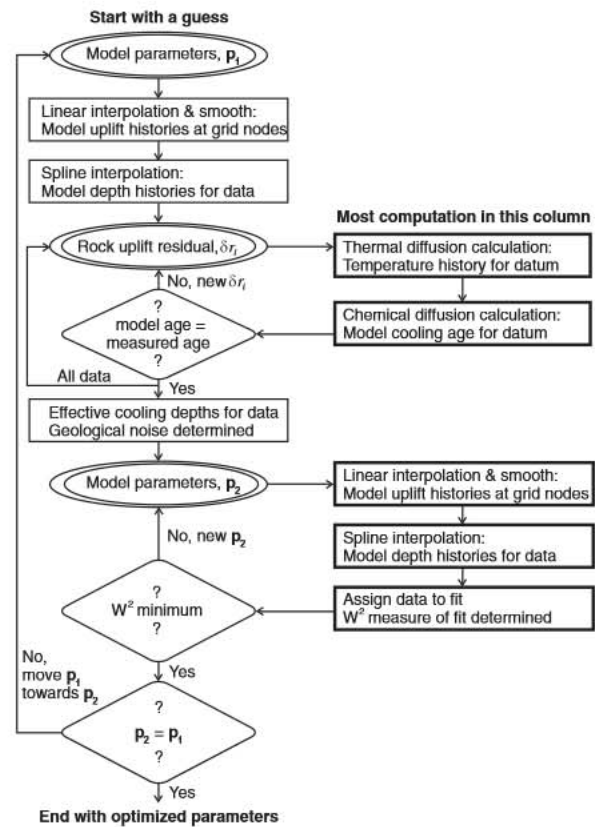
value at 5 Ma. A continuous rock uplift history is produced by linear interpolation and then smoothed by recomputing the gradient over a 5 My window of width (Fig. 9). Each rock uplift history starts at 80 Ma and is constrained not to allow burial (subsidence). Full details of the regression scheme and inference of confidence limits are given in Appendix 1.

The scheme that we choose to implement is purposefully naive with regard to boundary conditions that we impose. This is because our primary objective is to identify the general pattern of rock uplift that our data demand, rather than impose a spatially and temporally variable set of boundary conditions that we expect will correlate with the exhumation and cooling signal that we can measure. The sensitivity of our model and hence conclusions to more realistic boundary conditions are discussed after presentation of our results.

## RESULTS: SPATIAL AND TEMPORAL PATTERNS OF UPLIFT

The maximum rock uplift during the time of interest (younger than 34 Ma) was in northern Fiordland, where ~15 km of uplift is inferred (Fig. 10); peak temperatures were higher than the zircon annealing temperature of ~260 °C (Tagami, 2005), and close to the K/Ar white
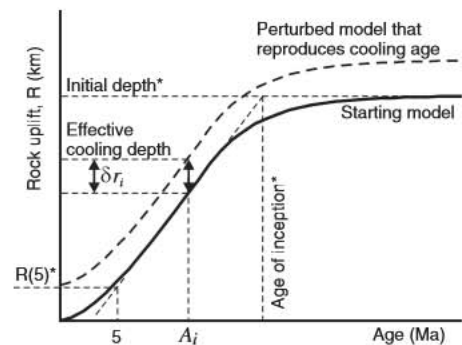


Figure 9. Graph illustrating how the starting model is constructed from three parameters (marked with asterisk): initial depth, age of inception, and the rock uplift since 5 Ma. The model is perturbed until the model and observed ages are equal, and hence rock uplift residual and effective cooling depth are determined.

mica closure temperature of ~350 °C (Dodson, 1973; Hames and Bowring, 1994). Farther southwest in coastal Fiordland, total rock uplift reduces to ~12 km between Doubtful Sound and Dusky Sound (Fig. 10), where a zircon partial annealing zone meets the coast. The southeastern margin of Fiordland has undergone only
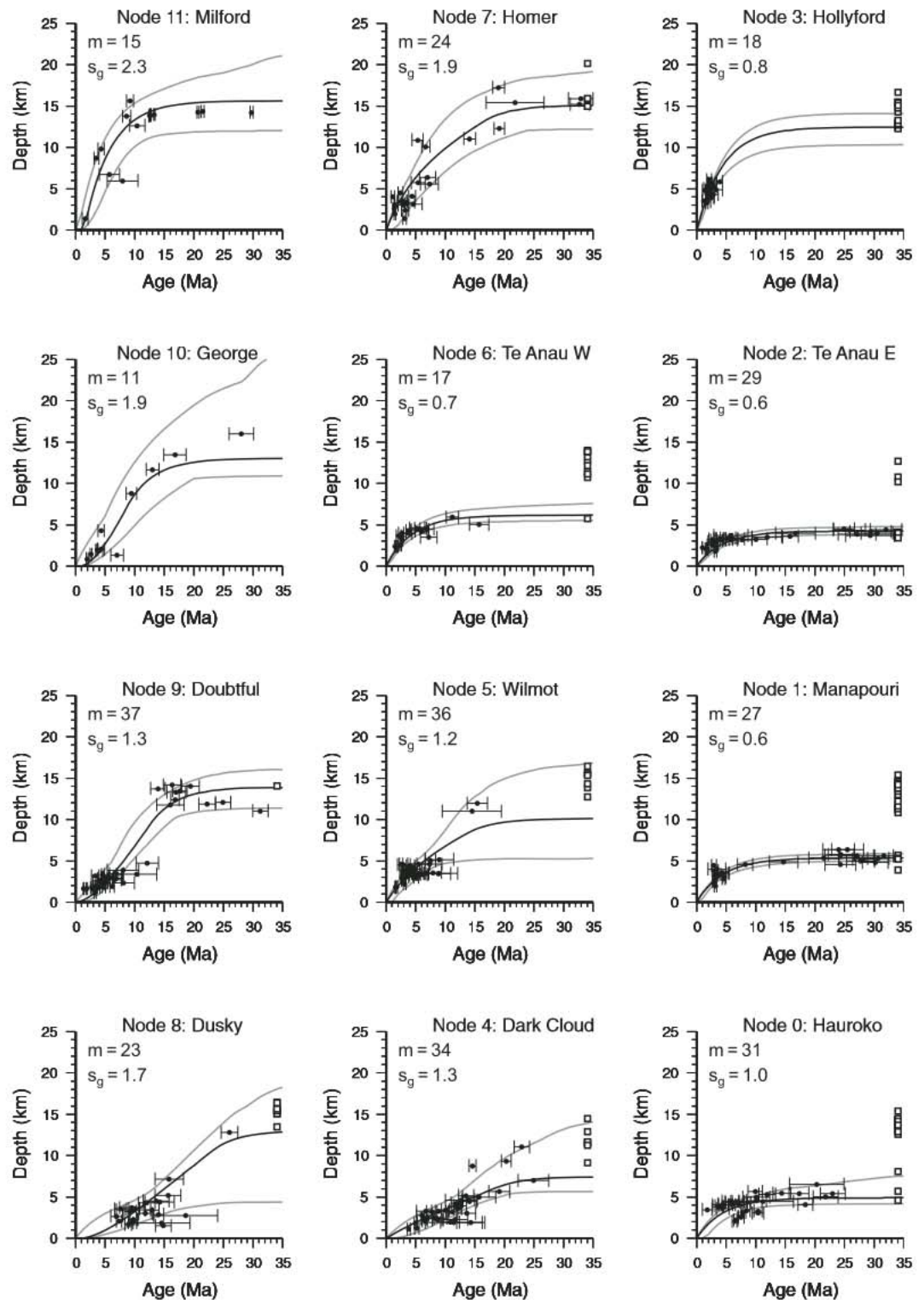
Figure 10. Results for each node (for locations see Fig. 4) of the optimized model. Observed ages with 95% uncertainties, and the 95% uncertainty in the best model (as determined from a chi-square statistic; Appendix 1) are shown. The number of data (m) constraining the node and the geological noise ($s_g$) value (km) for each node is also shown.

~4–5 km of uplift during the time of interest (Fig. 10), approximately corresponding to exhumation from the annealing depth for apatite fission tracks.

The onset of rapid uplift was later toward the northeast of the northwestern (Alpine fault) margin of Fiordland (Fig. 10). Uplift started near Dusky sound during the interval 25–15 Ma; reached a maximum near Doubtful Sound during the interval 15–10 Ma; continued to migrate past George Sound during the interval 10–5 Ma; and has been most intense near Milford Sound during the interval 5–0 Ma (Fig. 11; Animations 1 and 2). As the zone of maximum uplift rate spread northeast, a wave of increased uplift rate also spread eastward across Fiordland during the interval 10–0 Ma (Fig. 11). Optimal models for southwestern nodes at Dusky Sound and Doubtful
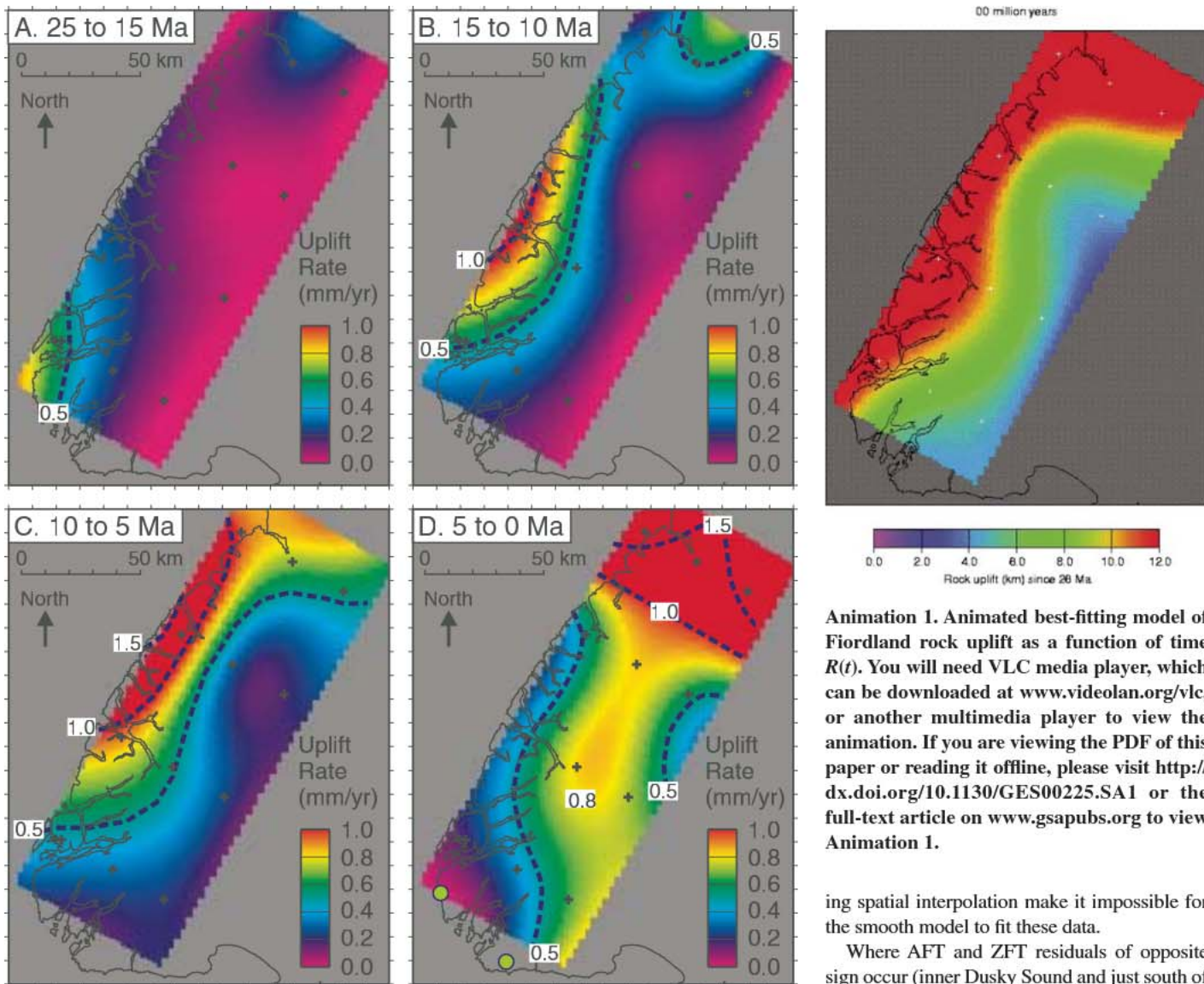
Figure 11. Uplift rates inferred during evolution of the Fiordland subduction zone.



Animation 1. Animated best-fitting model of Fiordland rock uplift as a function of time $R(t)$. You will need VLC media player, which can be downloaded at www.videolan.org/vlc, or another multimedia player to view the animation. If you are viewing the PDF of this paper or reading it offline, please visit http://dx.doi.org/10.1130/GES00225.SA1 or the full-text article on www.gsapubs.org to view Animation 1.

Sound predict that uplift rates have reduced during the past 5 My, but the difference in rate is barely significant, or is not significant (Fig. 10).
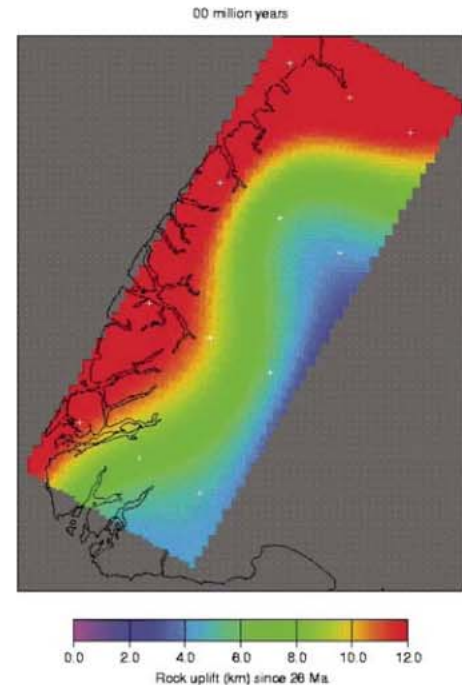
Model ages are predicted for every point on the existing topographic surface (Fig. 12), and the inferred thermal structure of the shallow crust (0–1 km below sea level) has a zone of elevated geothermal gradients where Pliocene–Quaternary uplift rates are predicted to be highest (Fig. 13).

## MODEL UNCERTAINTY AND GEOLOGICAL NOISE

The confidence limits shown in Figure 11 are based upon chi-squared tests and hence represent an estimate of the real range of rock uplift histories, because $\varepsilon_{ij}^2 \gg \sigma_i^2 + \sigma_j^2$ (equa-

tion 3; Fig. 6). In general, a model of tectonic stability followed by a phase of high uplift rate (~1 mm/yr) adequately fits most data (Fig. 10). However, spatial mismatch between the smooth model and geological reality is confirmed by examination of rock uplift residuals.

A systematic spatial correlation between rock uplift residuals is most clear for ZFT samples (Fig. 14): the optimum regional model of rock uplift systematically underestimates the true uplift for samples in an ~20-km-wide strip extending from the head of Dusky Sound to Milford Sound. A systematic spatial correlation is also observed for AFT samples in a 30-km-wide region south of Milford Sound, and in a region of 20 km width in the inner parts of Dusky Sound (Fig. 14). The 25:50 km node spacing and curvature limitation imposed dur-

ing spatial interpolation make it impossible for the smooth model to fit these data.

Where AFT and ZFT residuals of opposite sign occur (inner Dusky Sound and just south of Milford Sound; Fig. 14), then the model limitation of having only one possible inflection point at 5 Ma may also contribute to systematic misfit. A local region of rapid uplift at, for example, 20–10 Ma followed by a slower uplift rate cannot be fit using our chosen parameterization. It could also be that systematic inaccuracies associated with annealing or helium diffusion kinetics (e.g., related to rock type) could contribute to temporal misfit, even given a model with constant uplift rate.

The depth residuals from data that were used to constrain the rock uplift history are shown in Figure 15. Each residual is the vertical perturbation from the best-fitting regional rock uplift model that exactly reproduces the measured age at a sample site (Fig. 9). The combined set of residuals fits well a normal distribution with a mean of 0 km and standard deviation of 1.3 km (mean $s_g$ value). The most striking feature of the distribution of residuals is that there is a
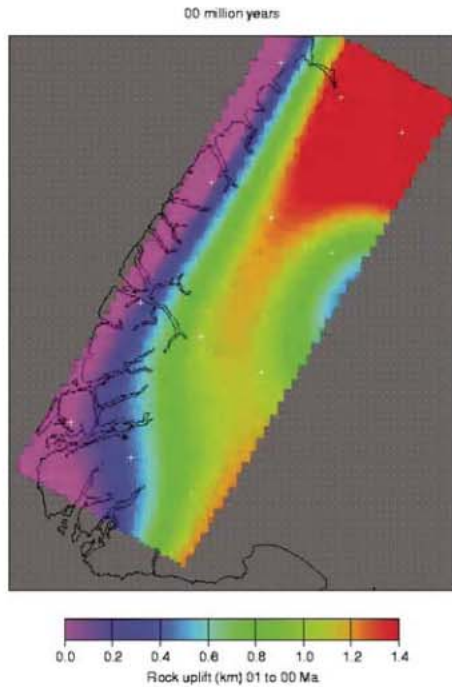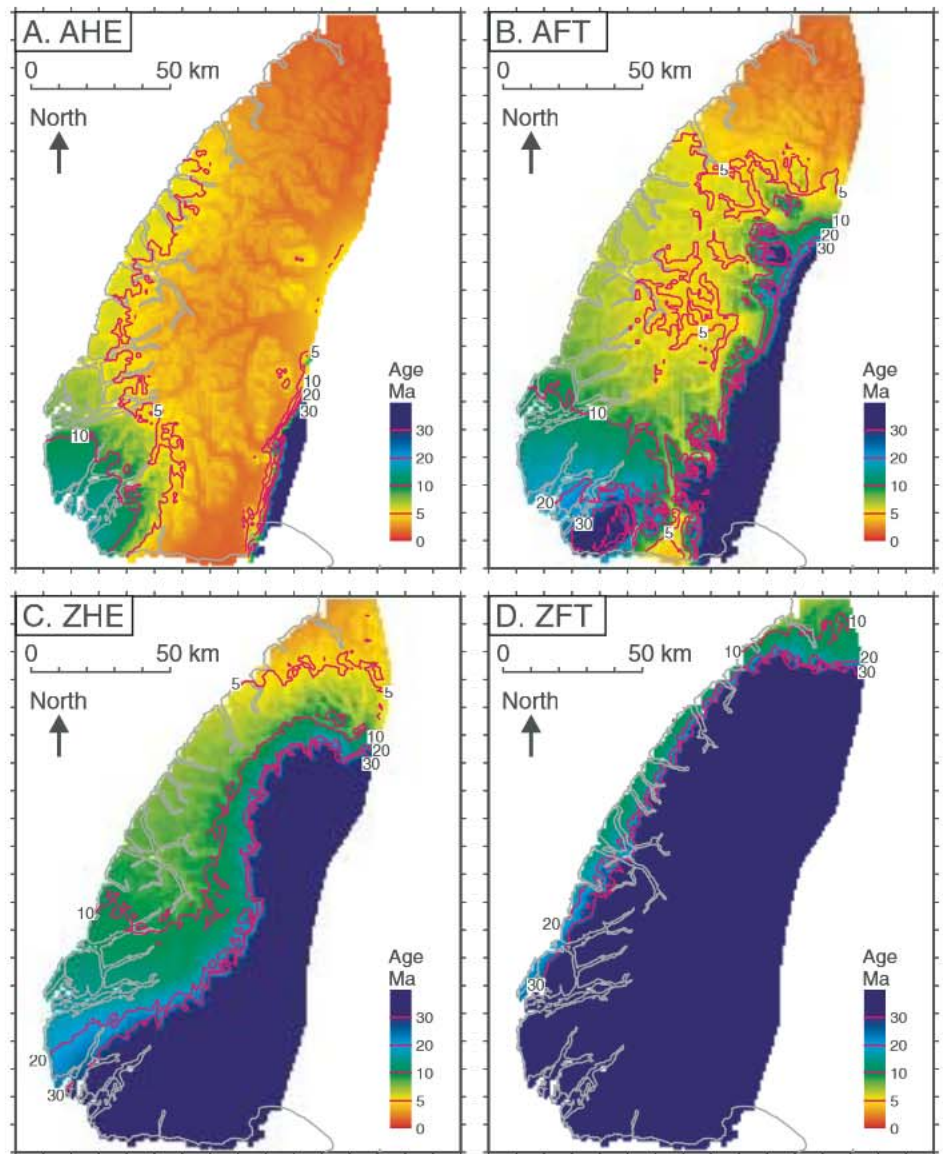
Animation 2. Animation model of Fiordland rock uplift rate as a function of time, $R'(t)$. You will need VLC media player or another multimedia player to view the animation. If you are viewing the PDF of this paper or reading it offline, please visit http://dx.doi.org/10.1130/GES00225.SA2 or the full-text article on www.gsapubs.org to view Animation 2.



Figure 12. Model ages for samples at the present topographic surface for each thermochronologic system. A) Apatite (U-Th)/He, AHE. B) Apatite fission track, AFT. C) Zircon (U-Th)/He, ZHE. D) Zircon fission track, ZFT.

systematic bias to positive residual values for systems with high closure temperature, and a slight bias toward negative residuals for systems with lower closure temperatures (Fig. 15). This bias is an inevitable consequence of the fact that low-temperature thermochronometers detect anomalously low exhumation histories, and high-temperature thermochronometers are biased toward anomalously high exhumation histories (see Fig. 16). We acknowledge that this introduces statistical bias into our modeling procedure, but reiterate that the combined residuals are approximately normally distributed.

The influence of faults is resolvable at a local scale in only a few instances. The clearest example is at the southern node (Lake Hauroko), where data clearly indicate a divergence in uplift trajectories: one path records rapid exhumation starting ca. 8–10 Ma, while the other path suggests a later onset ca. 2–4 Ma (Fig. 10, node 0). Examination of sample locations in the context of a geological map reveals that the variable signal is associated with exhumation on either side of the significant mapped Hauroko fault (Turnbull and Uruski, 1995).

Field mapping undertaken during this project and in other regional studies indicates that many brittle faults are recognizable in Fiordland, but no description of the regional pattern of brittle faulting has been published; many faults have only small throw, are difficult to recognize or trace over any significant distance, and kinematic indicators or offset markers are rare. Assuming a hypothesis that many brittle faults exist, our statistical consideration (section 3; Figs. 6 and 7) suggests that the accumulated throw on faults between sites spaced <10 km is in the range 0.5–3.3 km. The results of our best-fit model (Fig. 10) indicate consistent geological noise values in the range 0.6–2.3 km. These values represent accumulated throw on several

faults and include limitations imposed by model curvature, so individual fault throws are most likely to be lower than the values given above. Geotechnical data acquired during construction of the Manapouri tunnel, which is used to transport water from Lake Manapouri to Doubtful Sound (Fig. 4), confirm that the rock mass is pervasively fractured and faulted, with many recognizable faults at <1 km spacing.

## DISCUSSION OF MODEL ASSUMPTIONS

We adopt an objective but simplified approach to convert rock uplift histories into thermal histories and hence model ages. Specific issues
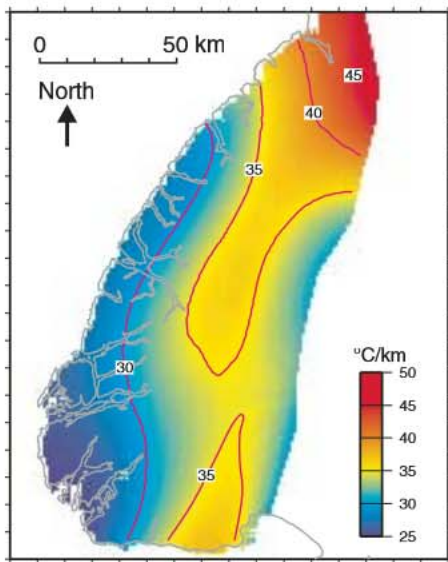
**Figure 13. Inferred geothermal gradient (°C/km) for the depth range 0–1 km below sea level. This result assumes a constant temperature of 10 °C at sea level, 760 °C at 30 km depth, and heat transport by thermal conduction and rock advection only. These assumptions are unlikely to be correct (see text).**



**Figure 14. Geographic distribution of rock uplift residuals: filled circles are values with magnitude <1 km; red filled triangles are values >1 km (burial was greater than the model predicts); inverted blue filled triangles are values <–1 km (burial less than model). Small squares are data that have ages too old to be relevant to the best model. Coastline is shown in gray. AHE—apatite (U-Th)/He; AFT—apatite fission track; ZHE—zircon (U-Th)/He; ZFT— zircon fission track.**
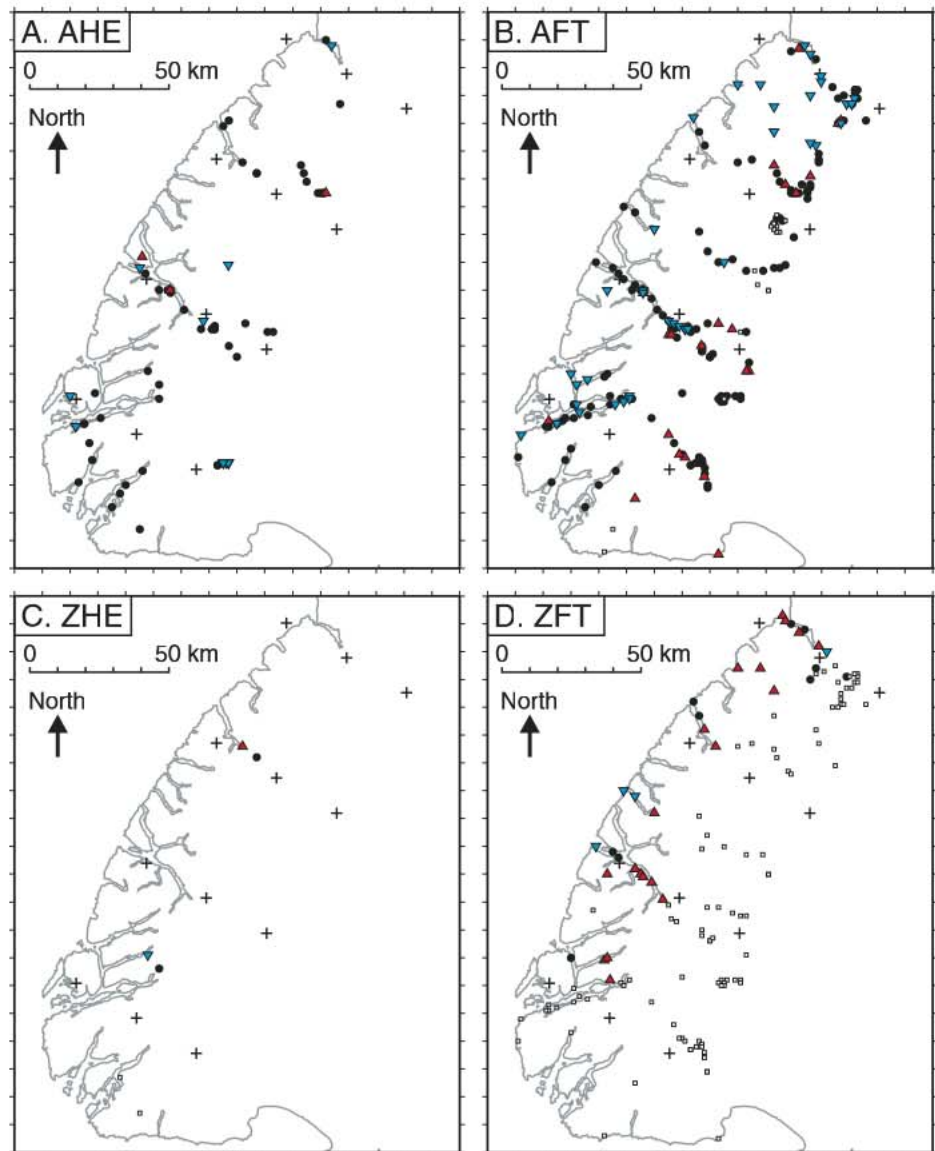
that require discussion are: initial conditions; heat productivity in the crust; the upper thermal boundary condition; edge effects caused by trench topography; and deformation of the lithosphere, particularly the effect of a subducted slab on the basal temperature boundary condition.

**Initial Conditions**

We assume a constant initial geothermal gradient that is consistent with that measured in nearby petroleum wells that are outside the zone of intense Cenozoic deformation (Funnell and Allis, 1996). Initial formation of the plate boundary through New Zealand in Eocene–Oligocene time was associated with minor rifting near Fiordland (Norris and Turnbull, 1993; Sutherland, 1995; Turnbull and Uruski, 1993), and may have perturbed the thermal structure of the lithosphere. The effect of locally raised heat flow values may cause our method to overestimate the total exhumation in some places, but we have no basis for imposing initial conditions that are other than uniform.

**Crustal Heat Production**

We ignore heat productivity within the crust, which in Fiordland is mainly composed of dioritic amphibolite or granulite gneisses that were exhumed from the lower crust during Creta-

ceous time (Clarke et al., 2000; Gibson and Ireland, 1995; Mattinson et al., 1986; Oliver, 1980). Based upon geochemical considerations, Fiordland crust is similar to or less radiogenic than that found in Taranaki Basin (Fig. 1), and hence contributes <18 mW m$^{-2}$ to the surface heat flow (Armstrong and Chapman, 1998). Heat productivity within the upper 5–15 km of crust, which is the part of interest, probably accounts for <10% of the background ~60 mW m$^{-2}$ of heat flow. We hence conclude that variations in crustal heat productivity are unlikely to

alter the geothermal gradient in the upper crust by more than ~1–2 °C km$^{-1}$; the perturbation caused by rock advection, which we model, is 5–20 °C km$^{-1}$ (Fig. 13). In addition, the effect is spatially uniform and introduces a comparable or smaller uncertainty than that of the initial conditions. Although this may affect absolute values of rock uplift, our conclusions are not likely to be affected because they are based upon the spatial pattern of rock uplift histories and are not sensitive to small differences in the total exhumation.
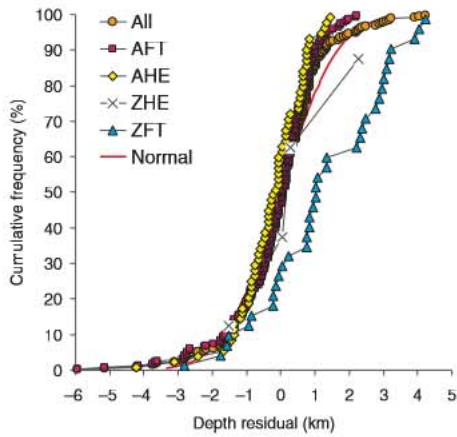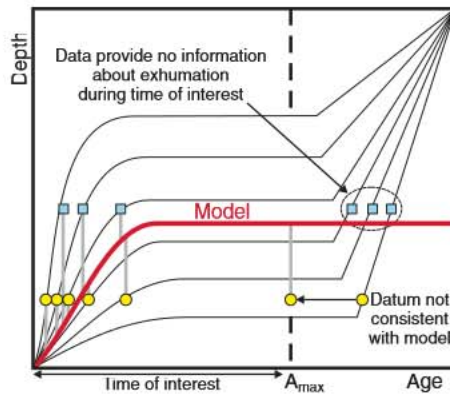
Figure 15. Cumulative frequency plot of rock uplift residuals for each thermochronologic system [AHE—apatite (U-Th)/He; AFT—apatite fission track; ZHE—zircon (U-Th)/He; ZFT—zircon fission track], the combined data set (all), and a reference normal distribution (normal) with mean 0 km and variance 1.3 km, which is the mean of the model values.



Figure 16. Diagram illustrating how different exhumation histories are sampled by different thermochonologic systems (blue filled squares versus yellow filled circles) and bias is introduced into the regression scheme. Systems with low closure-temperature sample shallow depths and even old ages place constraints on models that require greater burial. High-closure-temperature systems provide useful data for the anomalously deeply buried samples. *A* is age.



Figure 17. Temperature data measured close to sea level in the Manapouri tunnel, which traverses the central part of Fiordland (Fig. 4). Data from the western end of the tunnel are distinguished by open squares, and from the eastern end by filled diamonds. Y axis uncertainties show the range of surface elevations within a swath of width 1 km centered on the tunnel at the datum location; X axis uncertainties show a nominal measurement precision of 0.5 °C. A model conductive shallow temperature gradient of 20 °C/km is shown as a dashed line and clearly does not fit the data. The mean annual surface temperature (water inflow temperature at the surface) is shown dashed. Data from eastern and western ends of the tunnel cluster into distinct groups with moderate negative correlations between rock temperature and overburden. Water tunnel-inflow temperatures were measured and are consistent with measured rock temperatures.

## Surface Temperature and Topography Boundary Condition

We assume a constant upper temperature boundary condition at sea level that is close to the mean annual temperature. Our justification comes from rock and groundwater inflow temperature measurements made during construction of the Manapouri tunnel (Fig. 17), which show our assumption to be a good approximation in central Fiordland.

It is clear from Manapouri tunnel temperature data that groundwater efficiently removes heat from topographic anomalies, which have typical wavelengths of <10 km in Fiordland (Fig. 4), and maintains an almost constant rock temperature at sea level. We observe a greater effect in the western end of the tunnel, which is proximal to the Alpine fault and has greater total Cenozoic exhumation. It appears from the temperature data that the western end of the tunnel is hydrologically distinct from the eastern end, but both are strongly affected by groundwater heat advection (Fig. 17). We are undertaking an additional three-dimensional (3D) modeling study to fully evaluate the implications of data from the Manapouri tunnel.

In the European Alps, observations suggest that significant advection of heat by groundwater is unusual and limited to regions around confined fractured aquifers (Kohl et al., 2001; Marechal et al., 1999; Pastorelli et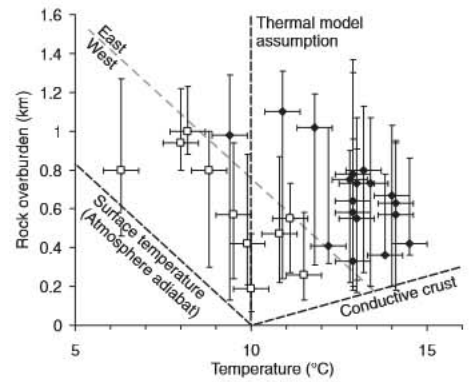 al., 2001). Hence, we suggest that Fiordland defines one end-member type of mountain range, because the rock mass is extensively fractured (above), there is no sediment or ice to seal the topographic surface, and the region has very high rainfall, which varies from 3.6 m/yr at Lake Manapouri to >8 m/yr on the mountain tops.

## Thermal Edge Effect

There is a topographic slope that falls ~4 km over a distance of ~20 km northwest of Fiordland, where the most western thrust faults deform and accrete basinal sediments (Figs. 1 and 5) (Barnes et al., 2002). The topographic slope and accretion of sediment along the northwest margin of Fiordland require lateral heat flow and will cause our model to overestimate temperatures at depth in the west. Present-day heat flow offshore along the northwest margin of Fiordland is ~40 mW m$^{-2}$, as inferred from bottom-simulating reflectors (Townend, 1997), significantly lower than the value of ~60 mW m$^{-2}$ determined from four petroleum exploration boreholes just east of Fiordland (Funnell and Allis, 1996).

## Basal Temperature Boundary Condition

We accept that the constant temperature boundary condition we assume at 30 km depth is naive, and is probably the most significant issue that makes our results unrealistic. We choose a simple and clearly stated basal boundary condition because it is objective and does not introduce any regional signal; it is our primary goal to recover the regional signal, so we do not want introduce circular reasoning by imposing a particular regional mechanical model.

There are two main issues that affect the realism of the lower boundary condition for our thermal model: emplacement of a slab in the mantle, and deformation within the crust. Whatever the reality, the thermal effects are insignificant to start, but become increasingly important as the deformation process continues. Fortunately, we are most interested in the start of the process, i.e., subduction initiation, so we contend that the time and place of initial cooling and the original depth are reliably determined (although see comments above).

Consider the effects of slab or crustal root emplacement on a particle that is initially in the middle crust at 5–15 km depth, the depth range in which we are interested. Both scenarios advect heat downward and lead to the lowering

of temperature gradients and temperatures in the middle crust. This cooling effect from below is in the same sense as that caused by the exhumation of rock from above. Hence, if our premise holds that both effects start at about the same time, then our model rock trajectories are likely to overestimate the rock uplift rates that immediately follow subduction initiation, and must correspondingly underestimate the most recent rock uplift. We suggest that this, in combination with edge effects, is a significant cause of the underprediction of Quaternary uplift rate at the western edge of Fiordland (Fig. 11), where uplifted marine terraces show the rate to be 0.5 mm/yr (Kim and Sutherland, 2004; Turnbull et al., 2007).

## IMPLICATIONS FOR SUBDUCTION INITIATION

### Spatial Evolution

The northeast migration of rapid exhumation and broadening of the exhumed zone have previously been suggested from consideration of a subset of the same data (House et al., 2002, 2005). We are now able to quantitatively track the development of this zone using the entire data set (Fig. 11; Animations 1 and 2) and estimate the total amount of exhumation. All directions referred to below are in the Pacific plate frame of reference.

The zone of maximum exhumation rate migrated northeast along the Alpine fault margin of Fiordland at ~1 cm/yr during the interval 20–5 Ma. This rate is ~30% of the relative plate motion rate (Fig. 18) and <50% of the Quaternary Alpine fault slip rate (Sutherland et al., 2006b). Therefore, we conclude that the signal is not caused by an initial condition associated with the geometry of the Australian plate and/or an asperity of the Alpine fault (Barnes et al., 2005; Sutherland et al., 2000). Instead, we suggest that Fiordland exhumation, inferred to be associated with elevated topography, was created in dynamic response to the twisting downward of the obliquely subducted slab. We propose that this zone of downward bending migrated northeast and spread out to the southeast as the overriding plate was internally shortened and tectonically eroded, and the slab increased in areal extent. The tectonic shortening and erosion of the overriding lithosphere have resulted in a lithospheric root with high seismic velocity (Eberhart-Phillips and Reyners, 2001), oroclinally bent basement geology (Norris, 1979; Sutherland, 1999), and a broad (250 km) zone of crustal thickening and mountain building to the north and east of Fiordland (Fig. 18). The coincidence of high-amplitude gravity and
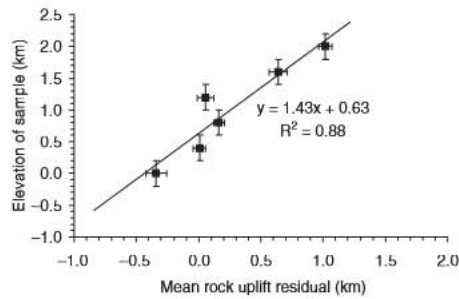


Figure 18. Graph showing the relationship between mean rock uplift residual and sample elevation for the entire data set of ages younger than 34 Ma (*n* = 302). Error bars for the Y axis (sample elevation) show the bin width of 0.4 km. Error bars for the X axis (mean rock uplift residual) are the standard error of the mean rock uplift residual in that bin. The number of data in each bin are (center, N): (0.0, 113), (0.4, 42), (0.8, 82), (1.2, 45), (1.6, 17), (2.0, 3).

topographic anomalies with the most tightly folded part of the subducted slab and the current zone of highest uplift rates in Fiordland (Fig. 11) lends support to our hypothesis that the topography and hence exhumation anomaly is primarily associated with inception and downward deflection of a slab.

As plate motion changed and total convergence increased through time, the subduction interface grew in extent. The zone of downward twisting migrated northeast and the southern tip-line of the subduction thrust migrated southwest. Stress levels are inferred to have been greatest at both these ends, consistent with the current locations of the highest-amplitude gravity anomalies (Fig. 2). It may also be that subduction of fracture zone weaknesses has influenced the geometry of the slab and overriding plate (Lebrun et al., 1998; Malservisi et al., 2003), or that membrane stresses within the slab have an additional effect (Reyners et al., 2002). The zone of subsidence that exists in the wake of the southward propagating subduction thrust tip may be due to some combination of the factors: tectonic erosion of the overriding plate; slab pull; loading of the overriding plate by elevated topography at the northern and southern ends of the zone; changes in bulk-rock or fault-rock physical properties through time, as total displacement increases; and an increase in age of the subducted slab and overriding plate through time—the subducting oceanic lithosphere is currently 40–20 Ma, but local convergence has occurred since 25–15 Ma. The last mechanism is an inevitable direct consequence of initiating subduction at a young fracture zone.

### Cause of the Exhumation Signal

Dynamic support of ~1–2 km of anomalous surface topography is predicted by numerical models to balance the integrated shear stresses associated with subduction initiation processes at depth (Toth and Gurnis, 1998). We acknowledge that more sophisticated 3D models will be required, but predict that a similar result will be found. We note that previous 3D models of Fiordland have suggested that a tear in the subducted slab may be necessary to explain the observed topography and gravity (Malservisi et al., 2003), but we suggest, based on observations from the Kermadec Trench (Billen and Gurnis, 2005), that a viable alternate possibility is that the elastic strength of the subducted lithosphere is much lower than that of intact lithosphere at the surface.

Assuming that a dynamic response of 1–2 km is physically reasonable, then it is expected that material will be removed by erosion from the elevated upper plate, and that an isostatic response to exhumation will restore the topography. In the absence of crustal strain this will cause the Moho to be advected upward. Using this reasoning, we previously calculated that the existing gravity and topography are consistent with ~7 km of crustal thinning, at which point an isostatic balance is reached. In central Fiordland (nodes 4–7), our data are broadly consistent with this hypothesis. However, we estimate 10–15 km of exhumation in western Fiordland (nodes 8–11).

The most likely explanation for the greater value of exhumation than expected from dynamic uplift alone is that crustal shortening has also occurred. Assuming an approximate width of the anomalous zone of 40 km, anomalous exhumation of 6 km, and initial crustal thickness of 30 km, a minimum shortening of ~8 km is calculated assuming conservation of crustal volume. This minimum value may significantly underestimate the true value of shortening if a conveyor of material is coming though the system along a dipping structure, as has been the case farther north along the Alpine fault (Walcott, 1998). However, the Alpine fault is a steeply dipping strike-slip fault with little or no Quaternary convergence across it adjacent to Fiordland (Barnes et al., 2005). Therefore, we conclude that the cause of the exhumation is primarily dynamic uplift associated with subduction initiation, but that there is a significant component of crustal shortening, especially in the west. We cannot rule out the possibility that the Alpine fault may have accommodated significant shortening adjacent to Fiordland during its Miocene phase of activity.

## SAMPLING STRATEGY AND ANALYSIS OF THERMOCHRONOLOGICAL DATA SETS

### Understanding the Evolution of Topography

A large body of published literature concludes that in many places the thermal structure of the upper crust is primarily controlled by conduction of heat, and hence low-temperature thermochronologic data can be used to directly derive information about the growth of finite-amplitude topographic anomalies (Braun, 2002; Kohl et al., 2001; Stuwe et al., 1994). However, data from the Manapouri tunnel (Fig. 17) demonstrate that there is no correlation between elevated sea-level temperatures and overlying mountainous topography in Fiordland. In fact, a negative correlation is found if data from the same hydrologic zone are considered. Hence, we conclude that it is not straightforward to determine any information about the evolution of individual topographic features in Fiordland using thermochronologic data. We have started a separate 3D modeling study to investigate what can be learned from the Manapouri tunnel data about the permeability of the crust, and further work is required to assess the viability of learning about topography development from thermochonologic studies in fractured and wet environments like that of Fiordland.

It may be that the onset of glaciation since 2 Ma has had some regional effect on our model by both cooling the rock mass (surface temperature boundary condition) and through enhanced erosion and hence exhumation. However, all of Fiordland has been heavily glaciated, so we might expect any effect to be uniform across the region and not affect the regional patterns in which we are most interested. In addition, most of the cooling ages that we model predate the onset of glaciation, so we expect the effect to be relatively minor. Our model is not designed to test hypotheses concerning changes in exhumation rate due to the onset of glaciation.

We note that there is a correlation and causal link in South Island between the long-wavelength (>50 km) topographic elevation, the local amplitude of short-wavelength (<20 km) topography, and the local exhumation rate. The strength of the correlation is modulated by regional factors such as the rock mass strength, precipitation, and proximity to the coast.

### Brittle Faulting, Rock Uplift, and the Estimation of Past Exhumation Rate

Age-elevation relationships have been widely used to constrain past exhumation rates (Benjamin et al., 1987; Fitzgerald, 1994; House et al., 2002, 1998). The principal assumptions required are that equal-cooling-age surfaces are close to horizontal now and when they were frozen into the rock, and that there are no faults between the sample sites. These may be valid assumptions or a useful approximation in many cases, especially where exhumation rates are low and uplift is driven by processes that do not involve widespread fault movement. However, we suggest that these assumptions do not hold true in an actively deforming obliquely convergent orogen with high upper crustal strain rates, as we find in Fiordland.

Age-elevation thermochronological transects require moderate or high topographic slopes, so that a range of elevations can be sampled as nearby as possible. However, it is well known that active faults produce fault scarps that may grow into mountains, and hence we expect fault locations to be spatially correlated with high topographic slopes and high elevations. Brittle fault zones, especially immature zones with relatively low total displacement (<2 km), are typically complex and composed of numerous strands with rotated blocks between them, or they are associated with zones of distributed folding. It is a significant problem that individual brittle faults are typically manifest at the surface as very narrow zones (<20 cm) that are preferentially eroded and covered by sediment and vegetation, and are hence difficult to identify from imperfect exposure in the field. We hypothesize that the steep locations that superficially seem best for age-elevation transects are affected in many places by brittle faults, and that it can be very difficult to demonstrate the existence of (or lack of) faults from field observations.

We did not design our sample strategy to resolve the details of local faulting, but we sampled several age-elevation transects, and attempted to collect nearby samples with maximum elevation difference in locations where it was practical to do so. When we compare age determinations from nearby (<1.5 km, <3.0 km), we find a poor positive correlation between age and elevation (Fig. 5). We suggest that this results from spatial variability between two competing effects: (1) erosion in the absence of local faults, and (2) active growth of reverse fault zones that lift rock more rapidly in their upthrown mountainous hanging wall. Effect 1 produces the conventional positive correlation between age and elevation, and effect 2 may produce a negative correlation if the difference in exhumation rate is sufficiently large across the reverse fault zone. Our proposal of numerous brittle faults in Fiordland with relatively small offset (<2 km) is consistent with field observations made by us and our colleagues, and with a detailed geotechnical study of the Manapouri tunnel; but we acknowledge that our data set is too sparse over most of the region to demonstrate the existence of any specific faults.

Our statistical analysis of age difference as a function of horizontal separation (Fig. 6) shows that within each thermochronological system there is a coherent regional horizontal age gradient that is likely controlled by lithospheric processes associated with the plate boundary. It is also clear from Figure 6 that the y axis intercept is resolved in the sense that differences in age between nearby samples are much greater than can be explained by analytical uncertainty. However, the intercept values (Fig. 6) do not distinguish between different reasons for local age variation (effects 1 and 2), and amalgamate data from many localities using an unrealistic (planar) function for the local geometry of age variation.

Our regression model provides an alternative measure of local short-wavelength brittle faulting around each grid node, because the regional exhumation model removes long-wavelength lithospheric-scale exhumation signals. The parameter $s_g$ (equation 8) is a summary statistic (standard deviation, km) that quantifies the misfit in rock uplift computed for localities closest to each node, and takes into account the age uncertainty. We suggest that offsets on local faults are a significant contributor, but acknowledge that spatial correlations between residuals (Fig. 14) imply some of the misfit is related to intermediate-wavelength signals that cannot be described by the small number of parameters we choose for the regional model.

Our regional model fits the data using conventional reasoning of subhorizontal isotherms at depth and uniform uplift, and predicts a positive age-elevation relationship everywhere. The result is that the rock uplift residuals have had the regional tectonic signal and the conventionally predicted age-elevation relationship removed. If the true rock uplift on mountains is higher than in valleys, because of the reverse faults that we hypothesize, then we would expect a positive correlation between rock uplift residuals and the elevation of the sample. In Figure 18 we analyze the rock uplift residuals from the regression, by binning them by elevation range of the sample, and then taking the mean value and standard error of each bin. The figure shows that there is a positive correlation, on average, when the entire data set is considered. However, the exact statistical meaning of Figure 18 is difficult to assess because we have amalgamated data of variable spatial density and closure temperature that have already been fit by a regression method. Our data set is barely dense enough to address this issue, and we do not have the computational resources to (marginally) improve our statistical

treatment (requires running the regressions many times to make predictions independent of the sample). We certainly cannot resolve details of individual faults around specific topographic features. However, on the basis of Figure 18, we conclude that there is a significant signal embedded in the residuals that is consistent with our hypothesis, and it could be investigated and quantified further.

## CONCLUSIONS

Our results enable us to track the progress of subduction initiation since 25 Ma in Fiordland, New Zealand. This is significant because there are few other places on Earth where it is possible to observe and analyze this process in such detail (Gurnis et al., 2004). We observe the onset of rapid exhumation at 25–15 Ma in southwest Fiordland, immediately following a time of significant change in regional plate motions (Cande and Stock, 2004). During the period 15–5 Ma, the locus of rapid exhumation broadened and migrated toward the northeast at ~30% of the plate motion rate, but exhumation remained localized along the northwest margin (Fig. 11). Since 5 Ma, the zone of rapid exhumation has become broader (expanded toward the southeast) and the present high-amplitude gravity and topographic anomalies are spatially associated with the most tightly folded part of the subducted slab.

We infer that the exhumation history tracks the development of topography, which is in turn related to the development of a through-going subduction interface and deflection of the nascent slab downward. The zone of subsidence southwest of Fiordland is in the wake of the southward-propagating subduction thrust tip. Subsidence may be due to a combination of factors such as tectonic erosion of the overriding plate, slab pull, loading of the overriding plate by elevated topography at the northern and southern ends of the zone, changes in bulk-rock or fault-rock physical properties through time, as total displacement increases, and an increase in age of the subducted slab and overriding plate through time. Oceanic lithosphere being subducted now has an age range of ca. 40–20 Ma, so it was very young during subduction initiation at 20 Ma.

We conclude that as plate motion changed and total convergence increased through time, the subduction interface grew in extent, a lithospheric root with high seismic velocity was formed to the northeast of the slab (Eberhart-Phillips and Reyners, 2001), and the crust of the overriding plate was shortened and bent into an orocline (Norris, 1979; Sutherland, 1999) (Fig. 19). The zone of downward twisting pro-
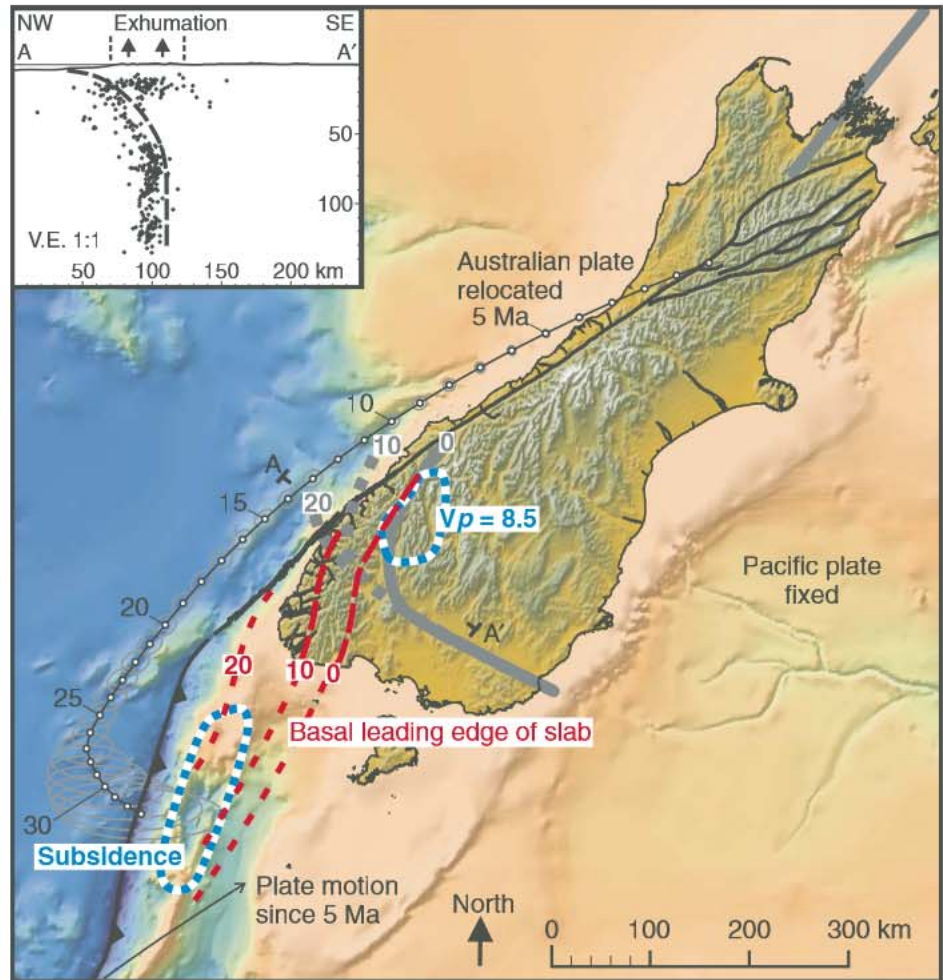


Figure 19. Shaded and colored digital-terrain model of South Island New Zealand (blue is deeper than 4 km). The trajectory of ellipses shows the interpolated position with 95% confidence of the Australian plate, relative to the Pacific plate, at 1 My intervals. The basement geology marker (bold gray) and its inferred locations at 10 Ma and 20 Ma are shown (dotted bold gray), along with the location of the lithospheric (100 km depth) high-seismic-velocity (V$p$ > 8.5 km/s) root (Eberhart-Phillips and Reyners, 2001). Deep seismicity is shown (inset) along the cross section marked A–A′ (Eberhart-Phillips and Reyners, 2001; Reyners et al., 2002). The zone of surface subsidence associated with the ridge above the subduction thrust is shown by the blue dotted line (see text). The leading basal edge of the subducted slab is shown as the red dashed line, along with the inferred locations at 10 Ma and 20 Ma. Deformation and tectonic erosion of the overriding Pacific plate has allowed the subduction zone to reach its current geometry from a zone of oblique collision along an early Miocene transform margin, resulting in an evolving uplift pattern in Fiordland and bending of South Island basement geology.

gressively migrated northeast and the southern tip-line of the subduction thrust migrated southwest. Stress levels are inferred to have been greatest at both these ends, consistent with the current locations of the highest-amplitude gravity anomalies (Fig. 2). Subduction of fracture zone weaknesses may have influenced the geometry of the slab and overriding plate (Lebrun et al., 1998; Malservisi et al., 2003), or

membrane stresses within the slab may have an additional effect (Reyners et al., 2002).

We find local positive correlations between age and elevation within our data set, and we find locations where the opposite is true. Data from the Manapouri tunnel show little variation in sea-level temperatures in highly fractured rock beneath high (>1 km) topography. We suggest that our observations are best explained by

brittle faults, and conclude that faulting can be significant during regional exhumation at temperatures <300 °C at active plate boundaries. We suggest that an entire population of brittle fault throws and block rotations is likely to exist in such settings, even if their existence is hard to prove. Faults may displace and rotate equal-cooling-age surfaces, and fractures increase rock permeability and encourage thermal perturbation of the upper crust by groundwater flow.

Our study highlights the importance of direct determination of past cooling rate on the same sample, or on very closely spaced samples with known field relations (outcrop rather than mountain scale), rather than relying on age-elevation relationships. A spatially complete and uniform sampling strategy is required to gain insight into the regional pattern of exhumation, which is controlled by lithospheric-scale processes, and the local controls of faulting on topography, where we expect causal relationships and spatial correlations between topographic features and fault locations. Our regression method, although naive in its assumptions, allows us to simultaneously consider the implications of all available data, evaluate summary statistics that describe the geological noise, and interpolate our regional exhumation model to make cooling age predictions that can be tested at any point. The residuals from our regression indicate that, on average (Fig. 18), mountain tops in Fiordland have undergone slightly greater rock uplift than adjacent valleys, even though we cannot identify specific faults.

## APPENDIX 1: REGRESSION METHOD TO DETERMINE REGIONAL ROCK UPLIFT HISTORY

### Rock Uplift History Parameterization at Each Node

The rock uplift since geological age $t$ at grid node $g$ is $R_g(t)$. We choose a parameterization for the rock uplift history that suits the hypotheses we wish to test. How much rock total rock uplift has occurred; when did uplift start; and how has the rate of rock uplift changed during the past 5 My? We require three parameters: an initial depth, an age of inception (older

than 5 Ma) for rock uplift and exhumation, and a rock uplift value at 5 Ma. A continuous rock uplift history is produced by linear interpolation and then smoothed by recomputing the gradient over a window of width 5 My (Fig. 9). Each rock uplift history starts at 80 Ma and is constrained not to allow burial (subsidence).

### Spatial Interpolation

We define a rectilinear grid of nodes that is appropriately oriented with respect to the Alpine fault (Fig. 4), which is the main crustal manifestation of the plate boundary and defines the northwest margin of Fiordland (Barnes et al., 2005). We choose a grid spacing of 50 km in a direction parallel to the Alpine fault, and 25 km perpendicular to the Alpine fault; the choice of distances yields an adequate number of data to fit at every node. For any specific age, the rock uplift value is smoothly interpolated at points other than the grid nodes, specifically datum locations, using natural bicubic splines.

### Thermal History Calculation and Effective Depth

A one-dimensional model is used because the perturbation of isotherms from the horizontal is minor at the relevant depths, as demonstrated by temperature measurements from the Manapouri tunnel (below) and from our previous three-dimensional models incorporating actual Fiordland topography (House et al., 2002). The model thermal history at each datum, $T_i(t)$, is calculated from the exhumation history using a one-dimensional Crank-Nicholson finite difference method with Dirichlet boundary conditions of constant sea-level temperature of 10 °C and a constant temperature of 760 °C at 30 km depth. We assume a constant initial geothermal gradient of 25 °C/km, which is consistent with heat-flow measurements from stable locations near Fiordland (Funnell and Allis, 1996); and a thermal diffusivity of $1.0 \times 10^{-6}$ $m^2 s^{-1}$, which is typical for high-grade metamorphic and igneous rocks similar to those in Fiordland (Clauser and Huenges, 1995; Vosteen and Schellschmidt, 2003).

The upper boundary condition leads to a definition of effective depth, $D_i(t)$, for datum $i$ at age $t$ as the model rock uplift value interpolated at the location of the datum, minus the elevation at the datum. This correction is for the constant temperature experienced during the rock uplift above sea level.

### Model Thermochronologic Ages

A model thermochronologic age, $A_i^*$, was calculated at each datum from $T_i(t)$. Apatite (U-Th)/He (AHE) and zircon (U-Th)/He (ZHE) ages were calculated using TERRA (Ehlers et al., 2005). Apatite fission track (AFT) and zircon fission track (ZFT) ages were calculated by a code (K. Gallacher, personal commun., 2003) that uses published annealing parameters for apatite (Laslett et al., 1987) and zircon (Tagami et al., 1998). K/Ar data are only relevant (ages within the range of interest) for the most northern node of our model, and there are only a few relevant data available (Claypool et al., 2002). Diffusion kinetic parameters for the white mica K/Ar system are not accurately known; we calculated model ages assuming a constant closure temperature of 350 °C (Dodson, 1973; Hames and Bowring, 1994), though we note that the mylonitic rocks sampled have been subjected to recrystallization at greenschist facies, which could cause us to slightly overestimate the temperature at which the measured age applies (Dunlap, 1997).

### Determination of Effective Cooling Depth

For each datum, the interpolated rock uplift history was perturbed by a fixed amount and the thermal history and model ages were recalculated (Fig. 9). A bisection scheme was used to find the value of the rock uplift residual, $\delta r_i$, which gives a model age equal to the measured age $A_i$.

Although the "closure" of a thermochronometric system occurs over a temperature range, it is useful to define an effective cooling depth for each datum

$$d_i = D_i(A_i) + \delta r_i \qquad (6)$$

This is an approximation for the depth, relative to sea level, at which the thermochronometric age was effectively frozen into the rock, and it is dependent on the cooling history.

### Treatment of Old Ages

If the cooling age of a datum is older than the maximum age of interest, $A_{max}$, then the age relates, at least in part, to events that occurred before the time of interest, and our chosen parameterization of exhumation history is likely to be inappropriate (Fig. 16). However, the datum places a constraint on the cooling history during the period of interest; the sample cannot have exceeded the closure temperature of the respective system during that time.

We treat old data ($A_i > A_{max}$) as follows: we redefine each old datum to the maximum age, i.e., $A_i = A_{max}$; we determine rock uplift residuals in the usual fashion, giving a model age equal to $A_{max}$; the rock uplift residual is only used to discriminate against models that are inconsistent with the datum (see definitions of quality-of-fit metrics below).

In our analysis, we consider the Oligocene-Holocene history ($A_{max} = 34$ Ma) as relevant to the process of subduction initiation beneath Fiordland, based upon published analyses of plate boundary motion (Cande and Stock, 2004; Sutherland, 1995) and local studies (Lebrun et al., 2003; Norris and Turnbull, 1993; Turnbull and Uruski, 1993).

### Estimate "Geological Noise"

Variance from the regionally smooth model of rock uplift history is introduced through known age uncertainty (measurement precision) and unknown geological noise associated with brittle faulting and block rotations. The expected value of the squared rock uplift residual at each datum is the sum of the geological variance, $s_g^2$, which we define independently for each grid node, $g$, and a fraction of the measured age variance $\sigma_i^2$ that depends upon the rate of rock uplift at the relevant time; and corrected for the fact that $p = 3$ model parameters have been adjusted to fit the $m_g$ pieces of data.

$$E\left[\left(d_i - D_i(A_i)\right)^2\right] = \frac{m_g - p}{m_g}\left(s_g^2 + \sigma_i^2 D_i'(A_i)^2\right) \qquad (7)$$

where

$$D_i'(A_i) = \left.\frac{\partial D_i(t)}{\partial t}\right|_{t=A_i}$$

Hence, we estimate the geological variance using:

$$s_g^2 = \frac{1}{m_g - p}\sum_{i=1}^{i=n}\gamma_{ig}'\left(d_i - D_i(A_i)\right)^2 - \frac{1}{m_g}\sum_{i=1}^{i=n}\gamma_{ig}'\sigma_i^2 D_i'(A_i)^2 \qquad (8)$$

and

$$m_g = \sum_{i=1}^{i=n} \gamma'_{ig} \qquad (9)$$

$\gamma'_{ig} = 1$ if $A_i < A_{max}$ (age within time of interest) and grid node $g$ is the closest to datum $i$; otherwise $\gamma'_{ig} = 0$.

## Determine Quality of Fit and Iterate to Find the Best Model

We define a weighted sum of squared residuals

$$W^2 = \sum_g \sum_{i=1}^{i=n} \frac{\gamma''_{ig}\left(d_i - D_i(A_i)\right)^2}{s_g^2 + \sigma_i^2 D_i'(A_i)^2} \qquad (10)$$

$\gamma''_{ig} = 1$ if grid node $g$ is the closest to datum $i$, and either $A_i < A_{max}$ or $\delta r_i < 0$ (datum not consistent with model, so use constraint; Fig. 16); otherwise $\gamma''_{ig} = 0$.

Each of the 12 nodes has 3 estimated parameters and a local evaluation of geological noise, so the number of degrees of freedom associated with $W^2$ is

$$f = \sum_g \sum_{i=1}^{i=n} \gamma''_{ig} - 48 \qquad (11)$$

We wish to find the set of parameters that minimizes $W^2$, but it is computationally prohibitive to recompute the model ages for each new set of parameters (about 1 hour of cpu time). To overcome this problem, we first perform a parameter search under the assumption that the effective cooling depth values $\{d_i\}$ are affected insignificantly by the slightly different shape of the new rock uplift model. This allows us to rapidly search the parameter space using a downhill simplex method (Nelder and Mead, 1965; Press et al., 2002) with multiple restarts to avoid local minima; hence we find a better set of parameters, toward which we then move part way. We then recompute the model ages and perform another parameter search. This process is repeated until no significant improvement to the model is realized (Fig. 8).

## Global Confidence for the Best-Fitting Regional Model

The procedure for finding the best-fitting model minimizes the estimated geological noise. We consider a null hypothesis that the estimated values of geological noise (equation 8) are the true values of geological noise. Our alternate hypothesis is that a new set of parameters, that defines a regional uplift model, is consistent with the same level of geological noise. We use the new weighted sum of squared residuals, $W_1^2$ (which has $f_1$ degrees of freedom), and the optimized value, $W_0^2$ (which has $f_0$ degrees of freedom), to define a test statistic

$$F = \frac{f_0 W_1^2}{f_1 W_0^2} \qquad (12)$$

Assuming that the test statistic is distributed as a (Fisher) F-distribution with $f_1 f_0$ degrees of freedom, then a 95% confidence region can be inferred from a one-tailed significance test. Using the actual values for our data set yields a definition of the 95% confidence region as any new set of parameters that satisfies $F < 1.222$. Our treatment of old ages may lead to a different number of degrees of freedom between the best and new model.

Unfortunately, it is not computationally feasible to fully explore the structure of the 36 parameter space

that defines the regional uplift model. It would also be a significant challenge to usefully communicate or visualize the results and covariation revealed by any such search. Instead, we consider an alternate simplified approach and explore the geological variability in exhumation history associated with each node independently (below).

## Nodal Confidence for the Best-Fitting Regional Model

We generate a synthetic data set of rock uplift values at each node by adding the rock uplift residuals for each datum nearest the node to the optimized model rock uplift values at the node at the measured age of the sample (synthetic data sets shown in Fig. 10):

$$r_{ig} = R_g(A_i) + \delta r_i \qquad (13)$$

We assume a null hypothesis that the optimized model is correct. Our alternate hypothesis is that a new set of 3 parameters that defines the rock uplift history at the node, with the same geological noise, can explain the observations at 5% significance level.

Without computing a new set of rock uplift residuals, we conduct a grid search through the 3 parameter space at the node and determine a weighted sum of squared residuals for each new model, $P_g(t)$:

$$Q_g^2 = \sum_{i=1}^{i=n} \frac{\gamma'''_{ig}\left(r_{i,g} - P_g(A_i)\right)^2}{s_g^2 + \sigma_i^2 R_g'(A_i)^2} \qquad (14)$$

where $\gamma'''_{ig} = 1$ if the grid node is closest to the datum and either $A_i < A_{max}$ or $P_g(A_i) > r_{ig} + \alpha s_g$; otherwise $\gamma'''_{ig} = 0$; $\alpha$ is the critical value at 95% confidence level of a Students t-distribution with $m_g$ degrees of freedom. This second condition utilizes old data where they may be a significant constraint. We assume that $Q_g^2$ is approximately chi-squared distributed with $l_g$ degrees of freedom, which is equal to the number of data used minus the 4 estimated parameters (includes the geological noise):

$$l_g = \sum_{i=1}^{i=n} \gamma'''_{ig} - 4 \qquad (15)$$

We use a grid search to find, for each node, an envelope of models that are not significantly different from the optimized model.

## REFERENCES CITED

Armstrong, P.A., and Chapman, D.S., 1998, Beyond surface heat flow: An example from a tectonically active sedimentary basin: Geology, v. 26, p. 183–186, doi: 10.1130/0091-7613(1998)026<0183:BSHFAE>2.3.CO;2.

Barnes, P., Davy, B., Sutherland, R., and Delteil, J., 2002, Frontal accretion and thrust wedge evolution under very oblique plate convergence: Fiordland Basin, New Zealand: Basin Research, v. 14, p. 439–466, doi: 10.1046/j.1365-2117.2002.00178.x.

Barnes, P.M., Sutherland, R., and Delteil, J., 2005, Strike-slip structure and sedimentary basins of the southern Alpine fault, Fiordland, New Zealand: Geological Society of America Bulletin, v. 117, p. 411–435, doi: 10.1130/B25458.1.

Benjamin, M.T., Johnson, N.M., and Naeser, C.W., 1987, Recent rapid uplift in the Bolivian Andes; evidence from fission-track dating: Geology, v. 15, p. 680–683, doi: 10.1130/0091-7613(1987)15<680:RRUITB>2.0.CO;2.

Billen, M.I., and Gurnis, M., 2005, Constraints on subducting plate strength within the Kermadec trench: Journal of Geophysical Research, v. 110, B05407, doi: 10.1029/2004JB003308.

Braun, J., 2002, Estimating exhumation rate and relief evolution by spectral analysis of age-elevation data-

sets: Terra Nova, v. 14, p. 210–214, doi: 10.1046/j.1365-3121.2002.00409.x.

Cande, S.C., and Stock, J.M., 2004, Pacific-Antarctic-Australia motion and the formation of the Macquarie Plate: Geophysical Journal International, v. 157, p. 399–414, doi: 10.1111/j.1365-246X.2004.02224.x.

Christoffel, D.A., and van der Linden, W.J.M., 1972, Macquarie Ridge–New Zealand Alpine fault transition: Antarctic Research Series, v. 19, p. 235–242.

Clarke, G.L., Klepeis, K.A., and Daczko, N.R., 2000, Cretaceous high-P granulites at Milford Sound, New Zealand; metamorphic history and emplacement in a convergent margin setting: Journal of Metamorphic Geology, v. 18, p. 359–374, doi: 10.1046/j.1525-1314.2000.00259.x.

Clauser, C., and Huenges, E., 1995, Thermal conductivity of rocks and minerals: American Geophysical Union Reference Shelf, v. 3, p. 105–126.

Claypool, A.L., Klepeis, K.A., Dockrill, B., Clarke, G.L., Zwingmann, H., and Tulloch, A., 2002, Structure and kinematics of oblique continental convergence in northern Fiordland, New Zealand: Tectonophysics, v. 359, p. 329–358, doi: 10.1016/S0040-1951(02)00532-2.

Collot, J.-Y., Lamarche, G., Wood, R., Delteil, J., Sosson, M., Lebrun, J.-F., and Coffin, M., 1995, Morphostructure of an incipient subduction zone along a transform plate boundary: Puysegur Ridge and Trench: Geology, v. 23, p. 519–522, doi: 10.1130/0091-7613(1995)023<0519:MOAISZ>2.3.CO;2.

Davey, F.J., and Smith, E.G.C., 1983, The tectonic setting of the Fiordland region, SW New Zealand: Royal Astronomical Society Geophysical Journal, v. 72, p. 23–38.

Delteil, J., Collot, J.-Y., Wood, R., Herzer, R., Calmant, S., Christoffel, D., Coffin, M., Ferriere, J., Lamarche, G., Lebrun, J.-F., Mauffret, A., Pontoise, B., Popoff, M., Ruellan, E., Sosson, M., and Sutherland, R., 1996, From strike-slip faulting to oblique subduction: a survey of the Alpine fault-Puysegur Trench transition, New Zealand, results of cruise Geodynz-sud leg 2: Marine Geophysical Researches, v. 18, p. 383–399, doi: 10.1007/BF00286086.

DeMets, C., Gordon, R.G., Argus, D.F., and Stein, S., 1994, Effect of recent revisions to the geomagnetic time scale on estimates of current plate motions: Geophysical Research Letters, v. 21, p. 2191–2194, doi: 10.1029/94GL02118.

Dodson, M.H., 1973, Closure temperature in cooling geochronological and petrological systems: Contributions to Mineralogy and Petrology, v. 40, p. 259–274, doi: 10.1007/BF00373790.

Dunlap, W.J., 1997, Neocrystallization or cooling? $^{40}Ar/^{39}Ar$ ages of white micas from low-grade mylonites: Chemical Geology, v. 143, p. 181–203, doi: 10.1016/S0009-2541(97)00113-7.

Eberhart-Phillips, D., and Reyners, M., 2001, A complex, young subduction zone imaged by three-dimensional seismic velocity, Fiordland, New Zealand: Geophysical Journal International, v. 146, p. 731–746, doi: 10.1046/j.0956-540x.2001.01485.x.

Ehlers, T.A., 2005, Crustal thermal processes and the interpretation of thermochronometer data: Reviews in Mineralogy and Geochemistry, v. 58, p. 315–350, doi: 10.2138/rmg.2005.58.12.

Ehlers, T.A., Chaudhri, T., Kumar, S., Fuller, C.W., Willett, S.D., Ketcham, R.A., Brandon, M.T., Belton, D.X., Kohn, B.P., Gleadow, A.J.W., Dunai, T.J., and Fu, F.Q., 2005, Computational tools for low-temperature thermochronometer interpretation: Reviews in Mineralogy and Geochemistry, v. 58, p. 589–622, doi: 10.2138/rmg.2005.58.22.

Fitzgerald, P.G., 1994, Thermochronologic constraints on post-Paleozoic tectonic evolution of the central Transantarctic Mountains, Antarctica: Tectonics, v. 13, p. 818–836, doi: 10.1029/94TC00595.

Funnell, R.H., and Allis, R.G., 1996, Hydrocarbon maturation potential of offshore Canterbury and Great South Basins, in 1996 New Zealand Petroleum Conference Proceedings: Wellington, New Zealand Ministry of Commerce, p. 22–30,

Gibson, G.M., and Ireland, T.R., 1995, Granulite formation during continental extension in Fiordland,

New Zealand: Nature, v. 375, p. 479–482, doi: 10.1038/375479a0.

Gurnis, M., Hall, C.E., and Lavier, L.L., 2004, Evolving force balance during incipient subduction: Geochemistry Geophysics Geosystems, v. 5, Q07001, doi: 10.1029/2003GC000681.

Hames, W.E., and Bowring, S.A., 1994, An empirical evaluation of the argon diffusion geometry in muscovite: Earth and Planetary Science Letters, v. 124, p. 161–167, doi: 10.1016/0012-821X(94)00079-4.

House, M.A., Wernicke, B.P., and Farley, K.A., 1998, Dating topography of the Sierra Nevada, California, using apatite (U-Th)/He ages: Nature, v. 396, p. 66–69, doi: 10.1038/23926.

House, M.A., Gurnis, M., Kamp, P.J.J., and Sutherland, R., 2002, Uplift in the Fiordland region, New Zealand; implications for incipient subduction: Science, v. 297, p. 2038–2041, doi: 10.1126/science.1075328.

House, M.A., Gurnis, M., Sutherland, R., and Kamp, P.J.J., 2005, Patterns of late Cenozoic exhumation deduced from apatite and zircon U-He ages from Fiordland, New Zealand: Geochemistry, Geophysics, and Geosystems, v. 6, Q09013, doi: 10.1029/ 2005GC000968.

Kim, K., and Sutherland, R., 2004, Uplift rate and landscape development in southwest Fiordland, New Zealand, determined using ${}^{10}$Be and ${}^{26}$Al exposure dating of marine terraces: Geochimica et Cosmochimica Acta, v. 68, p. 2313–2319, doi: 10.1016/j.gca.2003.11.005.

Kohl, T., Signorelli, S., and Rybach, L., 2001, Three-dimensional (3-D) thermal investigation below high Alpine topography: Physics of the Earth and Planetary Interiors, v. 126, p. 195–210, doi: 10.1016/ S0031-9201(01)00255-2.

Lamarche, G., and Lebrun, J.-F., 2000, Transition from strike-slip faulting to oblique subduction: Active tectonics at the Puysegur Margin, South New Zealand: Tectonophysics, v. 316, p. 67–89, doi: 10.1016/ S0040-1951(99)00232-2.

Lamarche, G., Collot, J.Y., Wood, R.A., Sosson, M., Sutherland, R., and Delteil, J., 1997, The Oligo-Miocene Pacific-Australia plate boundary, south of New Zealand: Evolution from oceanic spreading to strike-slip faulting: Earth and Planetary Science Letters, v. 148, p. 129–139, doi: 10.1016/S0012-821X(97)00026-5.

Laslett, G.M., Green, P.F., Duddy, I.R., and Gleadow, A.J.W., 1987, Thermal annealing of fission tracks in apatite 2. A quantitative analysis: Chemical Geology, v. 65, p. 1–13, doi: 10.1016/0009-2541(87)90189-6.

Lebrun, J.-F., Karner, G.D., and Collot, J.-Y., 1998, Fracture zone subduction and reactivation across the Puysegur ridge/trench system, southern New Zealand: Journal of Geophysical Research, v. 103, p. 7293–7313, doi: 10.1029/98JB00025.

Lebrun, J.-F., Lamarche, G., and Collot, J.-Y., 2003, Subduction initiation at a strike-slip plate boundary: The Cenozoic Pacific-Australian plate boundary south of New Zealand: Journal of Geophysical Research, v. 108, 2453, doi: 10.1029/2002JB002041.

Malservisi, R., Furlong, K.P., and Anderson, H., 2003, Dynamic uplift in a transpressional regime; numerical model of the subduction area of Fiordland, New Zealand: Earth and Planetary Science Letters, v. 206, p. 349–364, doi: 10.1016/S0012-821X(02)01100-7.

Marechal, J.C., Perrochet, P., and Tacher, L., 1999, Long-term simulations of thermal and hydraulic characteristics in a mountain massif: the Mont Blanc case study, French and Italian Alps: Hydrogeology Journal, v. 7, p. 341–354, doi: 10.1007/s100400050207.

Mattinson, J.M., Kimbrough, D.L., and Bradshaw, J.Y., 1986, Western Fiordland orthogneiss; Early Cretaceous arc magmatism and granulite facies metamorphism, New Zealand: Contributions to Mineralogy and Petrology, v. 92, p. 383–392, doi: 10.1007/BF00572167.

Melhuish, A., Sutherland, R., Davey, F.J., and Lamarche, G., 1999, Crustal structure and neotectonics of the Puysegur oblique subduction zone, New Zealand: Tectonophysics, v. 313, p. 335–362, doi: 10.1016/ S0040-1951(99)00212-7.

Nathan, S., Thurlow, C., Warnes, P., and Zucchetto, R., 2000, Geochronology database for New Zealand rocks (second edition): Institute of Geological & Nuclear Sciences Science Report 2000/11, 51 p.

Nelder, J.A., and Mead, R., 1965, A simplex method for function minimization: The Computer Journal, v. 7, p. 308–313.

Norris, R.J., 1979, A geometrical study of finite strain and bending in the South Island: Royal Society of New Zealand Bulletin, v. 18, p. 21–28.

Norris, R.J., and Turnbull, I.M., 1993, Cenozoic basins adjacent to an evolving transform plate boundary, southwest New Zealand, *in* Ballance, P.F., ed., South Pacific sedimentary basins: Sedimentary basins of the World 2: Amsterdam, Elsevier Science Publishers B.V., p. 251–270.

Oliver, G.J.H., 1980, Geology of the granulite and amphibolite facies gneisses of Doubtful Sound, Fiordland, New Zealand: New Zealand Journal of Geology and Geophysics, v. 23, no. 1, p. 27–41.

Pastorelli, S., Marini, L., and Hunziker, J., 2001, Chemistry, isotope values ($\delta D$, $\delta^{18}O$, $\delta^{34}S_{SO_4}$) and temperatures of the water inflows in two Gotthard tunnels, Swiss Alps: Applied Geochemistry, v. 16, p. 633–649, doi: 10.1016/S0883-2927(00)00056-1.

Press, W.H., Teukolsky, S.A., Vetterling, W.T., and Flannery, B.P., 2002, Numerical recipes in C++: The art of scientific computing (second edition): Cambridge, UK, Cambridge University Press, 1002 p.

Reay, A., and Parkinson, D., 1997, Adakites from Solander Island, New Zealand: New Zealand Journal of Geology and Geophysics, v. 40, p. 121–126.

Reyners, M., Robinson, R., Pancha, A., and McGinty, P., 2002, Stresses and strains in a twisted subduction zone—Fiordland, New Zealand: Geophysical Journal International, v. 148, p. 637–648, doi: 10.1046/j.1365-246X.2002.01611.x.

Stuwe, K., White, L., and Brown, R., 1994, The influence of eroding topography on steady-state isotherms. Application to fission track analysis: Earth and Planetary Science Letters, v. 124, p. 63–74, doi: 10.1016/ 0012-821X(94)00068-9.

Sutherland, R., 1995, The Australia-Pacific boundary and Cenozoic plate motions in the SW Pacific; some constraints from Geosat data: Tectonics, v. 14, p. 819–831, doi: 10.1029/95TC00930.

Sutherland, R., 1999, Cenozoic bending of New Zealand basement terranes and Alpine fault displacement: A brief review: New Zealand Journal of Geology and Geophysics, v. 42, p. 295–301.

Sutherland, R., Davey, F., and Beavan, J., 2000, Kinematics of plate boundary deformation in South Island, New Zealand, is related to inherited lithospheric structure: Earth and Planetary Science Letters, v. 177, p. 141–151, doi: 10.1016/S0012-821X(00)00043-1.

Sutherland, R., Barnes, P.M., and Uruski, C., 2006a, Miocene–Recent deformation, surface elevation, and volcanic intrusion of the overriding plate during subduction initiation, offshore southern Fiordland, Puysegur margin, southwest New Zealand: New Zealand Journal of Geology and Geophysics, v. 49, p. 131–149.

Sutherland, R., Berryman, K., and Norris, R.J., 2006b, Quaternary slip rate and geomorphology of the Alpine fault: Implications for kinematics and seismic hazard in southwest New Zealand: Geological Society of America Bulletin, v. 118, p. 464–474, doi: 10.1130/ B25627.1.

Tagami, T., 2005, Zircon fission-track thermochronology and application to fault studies: Reviews in Mineralogy and Geochemistry, v. 58, p. 95–122, doi: 10.2138/ rmg.2005.58.4.

Tagami, T., Galbraith, R.F., Yamada, R., and Laslett, G.M., 1998, Revised annealing kinetics of fission tracks in zircon and geologic implications, *in* Van den Haute, P., and De Corte, F., eds., Advances in fission-track geochronology: Dordrecht, Netherlands, Kluwer Academic Publishers, p. 99–112.

Toth, J., and Gurnis, M., 1998, Dynamics of subduction initiation at pre-existing fault zones: Journal of Geophysical Research, v. 103, no. B8, p. 18,053–18,067, doi: 10.1029/98JB01076.

Townend, J., 1997, Estimates of conductive heat flow through bottom-simulating reflectors on the Hikurangi and southwest Fiordland continental margins, New Zealand: Marine Geology, v. 141, p. 209–220, doi: 10.1016/S0025-3227(97)00073-X.

Turnbull, I.M., Sutherland, R., Beu, A.G., and Edwards, A.R., 2007, Pleistocene glaciomarine sediments of the Kisbee Formation, Wilson River, southwest Fiordland, and some tectonic and paleoclimatic implications: New Zealand Journal of Geology and Geophysics, v. 50, no. 3, p. 193–204.

Turnbull, I.M., and Uruski, C.I., 1993, Cretaceous and Cenozoic sedimentary basins of western Southland, South Island, New Zealand: Wellington, New Zealand, Institute of Geological & Nuclear Sciences Monograph 1, 86 p.

Turnbull, I.M., and Uruski, C.I., 1995, Geology of the Monowai-Waitutu area: Lower Hutt, Institute of Geological & Nuclear Sciences Geological Map 19, 68 p., scale 1:50000.

Vosteen, H.-D., and Schellschmidt, R., 2003, Influence of temperature on thermal conductivity, thermal capacity and thermal diffusivity for different types of rock: Physics and Chemistry of the Earth, v. 28, p. 499–509.

Walcott, R.I., 1998, Modes of oblique compression: Late Cenozoic tectonics of the South Island of New Zealand: Reviews of Geophysics, v. 36, p. 1–26, doi: 10.1029/97RG03084.

Wood, R.A., Lamarche, G., Herzer, R.H., Delteil, J., and Davy, B., 1996, Paleogene seafloor spreading in the southeast Tasman Sea: Tectonics, v. 15, p. 966–975, doi: 10.1029/96TC00129.